AIMS Materials Science, 13(3): 444–473.
DOI: 10.3934/matersci.2026022
Received: 11 December 2025
Revised: 16 April 2026
Accepted: 28 April 2026
Published: 26 May 2026

https://www.aimspress.com/journal/Materials

Research article

Ultrasound-assisted finishing of cellulosic textiles with silver/PVP nanoparticles: Effects of autoclave sterilization on antibacterial performance, nanoparticle release, and cytocompatibility

Nataly Arrieta-Sandoval, Claudia A. Rodríguez-González, Imelda Olivas-Armendáriz, Laura E. Valencia-Gómez and Juan F. Hernández-Paz*

Instituto de Ingeniería y Tecnología, Universidad Autónoma de Ciudad Juárez. 450 Del Charro Av., 32310, Juárez, Chihuahua, México

* **Correspondence:** Email: juan.hernandez.paz@uacj.mx; Tel: +52-656-2361187.

Abstract: The growing clinical demand for antimicrobial textiles requires ensuring that their performance remains stable after sterilization, a critical condition for medical-grade materials. Silver nanoparticles (Ag NPs) are widely used for their antimicrobial properties. However, autoclave sterilization can induce morphological and physicochemical changes due to wet steam and high-pressure conditions, potentially compromising their antibacterial performance. The specific behavior of polyvinylpyrrolidone (PVP)-stabilized Ag NPs immobilized on cellulosic fibers under clinically relevant sterilization conditions remains poorly understood. This study evaluated the antibacterial performance of Ag/PVP-coated cotton gauzes subjected to a standard clinical sterilization protocol consisting of autoclaving at 121 °C for 35 min followed by dry heating. The non-woven cotton gauzes were in situ impregnated with Ag/PVP nanoparticles under different synthesis conditions, with varying impregnation time and substrate alkalinity, with an emphasis on sonication as the dispersion method. The textiles were characterized by scanning electron microscopy (SEM), energy-dispersive X-ray spectroscopy (EDX), X-ray diffraction (XRD), and Fourier-transform infrared spectroscopy (FTIR), while colloidal solutions were analyzed by ultraviolet-visible spectroscopy (UV-Vis). Water absorption, water vapor permeability, and tensile properties were also evaluated. Quantitative evaluation of the antimicrobial effect of Ag/PVP nanoparticle-impregnated gauzes before and after the autoclaving process was performed according to ASTM E-2149 and correlated with nanoparticle size changes. Additionally, cell viability was evaluated using the 3-(4,5-dimethylthiazol-2-yl)-2,5-diphenyltetrazolium bromide (MTT) assay. Antibacterial testing according to ASTM E-2149 showed

reductions of approximately 95% against *Staphylococcus aureus* and 99% against *Escherichia coli*, which were maintained after autoclave sterilization. MTT results showed acceptable cell viability at 24 h, followed by a decrease at 48 h, indicating a time-dependent cytotoxic effect. The release study further revealed that an additional 24 h of static impregnation significantly improves nanoparticle homogeneity and release control. Overall, this work provides practical guidelines for the rational design of clinically compatible antimicrobial textiles with predictable post-sterilization behavior.

Keywords: antibacterial textiles; Ag/PVP nanoparticles; autoclave sterilization; release study

1. Introduction

Since ancient Egyptian times [1], cotton has been widely used for its absorbency, abundance, and relatively low cost, making it one of the most basic natural fibers in the textile industry [2]. From its earliest uses to the present day, cotton has been used for basic applications. However, its hydrophilicity can increase moisture retention and the risk of bacterial proliferation, which can cause infection [3]. Thus, there has been a need to develop functional textiles, such as antimicrobial textiles [4], that can also serve as a substrate for the adsorption of drugs and active substances [5].

In the field of functional textiles, the use of nanomaterials, such as certain nanoparticles of metallic elements like gold [6–8], platinum [9], copper [10,11], and silver [12,13], has made it possible to manufacture composites based on cotton and other cellulosic substrates with improved properties. These nanostructures, adsorbed on their fibers, act as active agents that impart the new properties to the textile. Among them, silver nanoparticles have been shown to have antimicrobial, antiviral, and antifungal action, making them one of the most widely used nanostructures in the development of functional textiles [14]. Their application ranges from the preparation of hydrogels [15–18] and nanofibers [19–21] to their incorporation in synthetic [22–25] and natural fibers, such as cellulosic fibers, including cotton. Recent studies have further reinforced the relevance of silver-based antimicrobial materials in biomedical applications. For example, silver-loaded viscose fabrics have shown durable antibacterial performance, highlighting the continued interest in cellulosic textile substrates for functional medical materials. In parallel, more recent bio-based Ag nanostructures, such as lignin/Ag nanoparticle systems with spiky surface features, have demonstrated combined antibacterial and antioxidant functionality, reflecting the current trend toward multifunctional and sustainable antimicrobial platforms [26,27]. Currently, several textile products for medical use already integrate silver nanocrystals in their structure: Puracol®Plus (using collagen substrate), Acticoat™ (polyethylene substrate), Promogran Prisma® (collagen and regenerated cellulose substrate), Suprasorb®A + Ag (calcium alginate substrate), Silverlon® (nylon substrate), and Aquacel® Ag (cellulose substrate), among others [28].

In situ synthesis/impregnation of metal nanoparticles from textiles by metal reduction in solution involves generating silver nanoparticles directly on cellulosic fibers previously loaded with metal ions, instead of synthesizing them and then depositing them on the fibers. Throughout the synthesis of colloidal nanoparticles (especially those of metallic composition), it is required to incorporate a stabilizing agent to keep the nanoparticles dispersed in the solution and avoid agglomeration/precipitation. This agent confers hydrophilicity, improves solubility in aqueous media, and modulates the size of the particles formed. Among the most widely used stabilizers,

polyvinylpyrrolidone (PVP) stands out. This is a synthetic, water-soluble polymer that, thanks to its structure, can form complexes with ions such as metals, which explains its wide application in the colloidal synthesis of metallic nanostructures [29–31]. Another important advantage of PVP is its biocompatibility, an essential feature for medical applications [32,33].

The approach of performing in situ impregnation of textiles during metal reduction, combined with the use of ultrasound as a means of agitation and dispersion of the molecules, favors a more homogeneous distribution of the nanoparticles on the cellulosic fibers. The propagating high-frequency acoustic waves (~20–40 kHz) generate and collapse microbubbles in the medium (cavitation); this violent breakup of the microbubbles creates transient microenvironments of elevated temperature and pressure. This localized energy, especially at the textile–solution interface, optimizes mass transfer in the inter- and interfibrillar pores of the yarn [34–36]. Therefore, the application of ultrasound has been widely investigated in the textile industry for pretreatment processes, such as impurity removal [37], coloration [38], and in textile finishes to provide specific properties to the material, such as antimicrobial activity [39,40], UV blocking [41], and antistatic effects [42].

For materials with antibacterial function, it is essential that this function is maintained after sterilization, with sterilization being understood as the total elimination of viable microorganisms, including bacterial spores [43]. Within the sterilization processes, the most accessible, safe, and effective sterilization process is autoclaving, a process in which the material to be sterilized is completely immersed in saturated water vapor at high pressure (121–125 °C for 15–30 min). These conditions of high pressure and temperature in a humid environment are critical variables to consider when sterilizing substrates with adsorbed nanoparticles, since the humid heat can induce aggregation, causing changes in the morphology and size of the nanoparticles, which would functionally affect their antibacterial effectiveness.

The choice of the stabilizing agent is a key factor to maintain the morphology of the nanoparticles at the time of autoclaving, since the temperature and pressure can partially degrade this coating and favor agglomeration and also a possible oxidation of the metallic nanostructures. For example, in membranes of polyvinyl alcohol (PVA) fibers manufactured by electrospinning doped with silver nanoparticles, antibacterial capacity was affected since the average particle size increased by ~247% [44]. In contrast, in citrate-stabilized colloidal silver nanoparticles (commercial), there was no colloidal particle size modification after the sterilization cycle, although it did show increased platelet aggregation in in vitro tests [45]. It is evident that the use of one or another coating dictates the behavior of the particles at the time of autoclaving; for example, A. Franca et al. showed that using polyethylene glycol (PEG) as a stabilizer in gold nanoparticles maintained the particle size, unlike using thiopronine as a coating, where particle agglomeration was observed [46]. Another important difference in the behavior of the nanoparticle-stabilizer system during the autoclaving cycle lies in the physical state they are in. Nanoparticles in liquid suspension (colloid) behave differently than when they are deposited in solid form on the dry substrate, as occurs in textiles with nanoparticles adsorbed on the surface of the fibers.

To the best of our knowledge, no previous studies have investigated the impact of autoclaving on the morphology, particle size, and antibacterial activity of Ag/PVP nanoparticles adsorbed on cellulosic substrates such as non-woven cotton medical gauze. Therefore, the objective of this study was to evaluate the stability, antimicrobial behavior, and biosafety of cotton gauze impregnated in situ with Ag/PVP nanoparticles before and after undergoing a standard clinical autoclave sterilization protocol, establishing the relationship between the synthesis conditions of the nanoparticles, their

response to the sterilization process, and their functional behavior. It is hypothesized that Ag/PVP nanoparticles immobilized on cotton fibers retain their morphological stability and antibacterial activity after autoclave sterilization, as the PVP shell provides sufficient protection to prevent significant structural or functional degradation under humid-heat conditions.

2. Materials and methods

2.1. Materials

Silver nitrate ($AgNO_3$, powder, purity ≥99.0%), polyvinylpyrrolidone (PVP, powder, 40k mw), sodium borohydride ($NaBH_4$, ≥98.0%), sodium chloride (NaCl, ≥99.0%), sodium hydrogen carbonate ($NaHCO_3$, ≥99.7%), potassium chloride (KCl, ≥99.0%), di-potassium hydrogen phosphate trihydrate ($K_2HPO_4 \cdot 3H_2O$, ≥99.0%), magnesium chloride hexahydrate ($MgCl_2 \cdot 6H_2O$, ≥99.0%), calcium chloride ($CaCl_2$, ≥97%), sodium sulfate (Na_2SO_4, ≥99.0%), Tris-hydroxymethyl aminomethane [$NH_2C(CH_2OH)_3$, ≥99.8%], hydrochloric acid (37% conc.), dimethyl sulfoxide (DMSO, CH_3SOCH_3, ≥99.5%) and MTT reagent (thiazolyl blue formazan, powder, ≥97.5%) were purchased from Sigma-Aldrich. Sodium hydroxide (NaOH, granules, ≥99.0%) was purchased from Kelve. DMEM medium (10-013-CV), bovine fetal serum (35-010-CV), and 96-well plates were purchased from Corning. The antibiotic penicillin-streptomycin was purchased from Gibco. Phosphate-buffered saline (PBS) was prepared in the lab. The 7.5 × 5.0 cm 100% cotton gauze pads were obtained from the Curapack brand. Distilled water was purchased from a local distributor; when sterilization was necessary, it was by autoclaving for 35 min at 121 °C (All American model 25×). The test microorganisms used were *Staphylococcus aureus* (ATCC®6538™) and *Escherichia coli* (ATCC® 11229™). The ultrasonic bath used in the impregnation process was the Cole-Parmer model 8893 with 40 kHz power.

2.1.1. Ethics approval of research

Primary fibroblasts were isolated from Balb/c mice after receiving approval from the Research Ethics Committee of the Universidad Autonoma de Ciudad Juarez, with the approval number CEI-2025-1-31, issued on February 25, 2025.

2.2. Preparation of textile Ag/PVP

2.2.1. Immersion of textile in NaOH solution

Four sterile gauzes were placed in 100 mL of NaOH solution (3 M) for 1 h at room temperature. The textile was rinsed with distilled water four times (gently squeezed and placed in successive glasses of distilled water with 150 mL in each glass). Then, the textile was pressed manually to extract the non-impregnated solution and placed in a covered container. This material is identified as *activated textile*.

2.2.2. In situ impregnation of the textile—experimental design of the impregnation time and ultrasonic dispersion

80 mL of water was poured into a beaker, and 800 mg of PVP were added. The water–PVP solution was kept at room temperature under magnetic stirring for 10 min. In a beaker, 20 mL of water and $AgNO_3$ powder (100 mg) were added; this beaker was placed for 15 s in an ultrasonic bath to disperse the salt in the water. The water–$AgNO_3$ mixture was added to the water–PVP mixture and stirred for 15 min in a magnetic stirrer. Subsequently, the textiles (four pieces of activated textile) were added to the water–PVP–$AgNO_3$ mixture, maintained without agitation for 30 min, and covered with aluminum foil. The $NaBH_4$ reducing solution was added by dripping for 1 min (prepared according to the required molarity in Table 1) and allowed to mix for 30 min in magnetic stirring at 100 rpm (sample 1). To observe the saturation and morphology of the nanoparticles adsorbed on the substrate, an additional 24 h of impregnation without agitation after reduction (sample 1 + 24 h) was applied, as well as performing synthesis in an ultrasonic bath (when adding the reducing solution, the reaction glass was immersed in the ultrasonic bath) to improve the dispersion of the particles on the substrate (sample 1 US). Impregnation was also performed for an additional 24 h in the ultrasound sample (1 US + 24 h) to allow greater impregnation of the Ag/PVP nanoparticles into the cellulosic fibers and to improve the uniformity of the coating.

Table 1. Experimental design. Variables: impregnation time and ultrasonic dispersion.

Sample	$AgNO_3$ (M)	Molar ratio: Ag/PVP	Molar ratio: $NaBH_4/AgNO_3$	Dispersion/agitation during reduction	Additional impregnation (24 h)
1	0.0059	29.43	1	Magnetic stirring	No
1 + 24 h				Magnetic stirring	Yes
1 US				Ultrasonic bath	No
1 US + 24 h				Ultrasonic bath	Yes

2.2.3. Experimental design of variables: alkalinity of the activated textiles

To observe the effect of the alkalinity of the activated textile on the morphology of the nanoparticles adsorbed on the textile, three values of pH (7.2, 9.3, and 11.5) were used (Table 2), using the sample preparation 1 in ultrasound. The pH value was measured for the residual water of the last washing beaker. After leaving four activated gauzes for 3 min in each beaker with occasional agitation, they were manually drained and left wet in a Petri dish to be used for synthesis the following day. The pH value of the impregnation of textiles in the water–$AgNO_3$–PVP solution after reduction in the ultrasonic bath was also recorded.

Table 2. Experimental design. Variables: alkalinity of activated textiles.

Sample	pH*	$AgNO_3$ (M)	Molar ratio: Ag/PVP	Molar ratio: $NaBH_4/AgNO_3$
1 US + 24 h 9.3	9.3	0.0059	29.43	1
1 US + 24 h 7.2	7.2			
1 US + 24 h 11.5	11.5			

*pH value of the residual water from the last rinse of textiles.

2.2.4. Washing and drying of the textile Ag/PVP

At the end of the reaction time, textiles were removed from the impregnation solution and rinsed three times with distilled water (100 mL each washing beaker) to remove the non-adsorbed species. Then, textiles were manually pressed to remove the remaining water and oven-dried at 80 °C for 2 h with the aid of a vacuum maintained at 0.06 MPa. This material, identified as textile Ag/PVP, was stored in a closed container protected from light.

2.2.5. Sterilization of textile Ag/PVP

Textiles were placed in sealed sterilization bags prior to autoclaving at 121 °C at 15 psi for 35 min using an All American autoclave, model 25×. After autoclaving, samples were heat-dried at 120 °C for 45 min while remaining inside the sealed bags.

2.3. Characterization

Morphology and chemical analysis [by energy dispersive X-ray spectroscopy (EDX)] of the materials were conducted using a Hitachi SU5000 scanning electron microscope. No preparation was required for the textiles; the material was simply cut for placement in the sample holders. Absorbance spectra of the liquid samples (textile Ag/PVP impregnation reaction solution diluted in distilled water) were obtained by a StellarNet spectrometer with model SL5 deuterium-halogen light source in the spectral range of 300–800 nm, using a quartz cell as the sample carrier. Infrared analysis in the attenuated total reflectance mode was carried out on a Nicolet 6700 equipment, in the range of 4000–600 cm^{-1} using 100 scans with 16 cm^{-1} resolution. A piece of textile Ag/PVP sample was folded and placed for analysis. The analysis of the crystalline state of the samples was carried out on a Panalytical X'pert Powder diffractometer with copper filament radiation.

2.4. Water absorption capacity

The dry textile was weighed (W_{dry}) and placed for 2 min in a beaker with 50 mL of distilled water. Samples were then removed and placed on a filter paper for 30 s to allow the excess water to come out, and then re-weighed (W_{wet}). For each sample, five independent repetitions were performed, and the mean values are reported. The water absorption percentage was calculated using Eq 1:

$$\text{Water absorption (\%)} = \frac{W_{\text{wet}} - W_{\text{dry}}}{W_{\text{dry}}} \times 100\% \quad (1)$$

2.5. Water vapor permeability

The ability to pass water vapor through the textile (at 37 °C) was evaluated by the water vapor permeability test. 37 °C was selected as the temperature to simulate physiological conditions relevant to the in vivo application of wound dressings. Three samples per textile type were each placed on a 50 mL beaker (diameter of 4.1 cm) with 40 mL of distilled water (water was added before placing the textile); the textile was fixed with a rubber band. The beaker (containing water, the textile sample, and the rubber band) was weighed and then kept in an oven at 37 °C for 24 h. After that, each beaker was removed and re-weighed. The permeability result was calculated by dividing the water loss (g) by the vapor passage area (m^2), and the mean value of the three independent repetitions is reported. The permeability value was calculated as Eq 2:

$$\text{Permeability} = \frac{\text{Water loss (g)}}{\text{Vapor transmission area (m}^2\text{)}} \quad (2)$$

2.6. Mechanical properties

The textiles were folded in half and subjected to a tension test at 5 mm/min in a Sintech universal machine model 20/D, with a fixed opening of 30 mm for all samples, testing four specimens for each sample type. The results of elongation (%) and breaking strength (MPa) are presented.

2.7. Evaluation of antimicrobial capacity

A quantitative antibacterial evaluation of the textile samples was carried out under ASTM-E2149 (with modifications), using *Escherichia coli* (ATCC® 11229™) and *Staphylococcus aureus* (ATCC® 6538™) as representative Gram-negative and Gram-positive strains, respectively, as recommended and commonly employed in this standard. Freshly formed bacterial broths were used (100 mL with an isolated colony collected from a recent seeding), with an incubation time of 19 h at 37 °C and diluted in sterile water to a concentration of 1.6×10^5 colony-forming units per milliliter (CFU/mL) (calibration curve estimation and verified by counting by seeding serial dilutions). Each textile sample was individually immersed in 20 mL of the corresponding bacterial suspension (*Staphylococcus aureus* and *Escherichia coli*) and kept for 2 h in the incubator at 37 °C, with shaking in the vortex for 15 s every 15 min. Subsequently, serial dilutions of 10^1, 10^2, and 10^3 were prepared, and 50 µL was spread in Petri dishes (90 mm diameter) in triplicate and kept in the incubator for 24 h at 37 °C. The bactericidal effect was determined from the decrease in CFU/mL compared to those observed in the control sample (sterile virgin gauze). The mean value of three independent repetitions is reported. The percent reduction was calculated using Eq 3:

$$\text{CFU reduction (\%)} = \frac{\text{CFU control} - \text{CFU sample}}{\text{CFU control}} \times 100\% \quad (3)$$

2.8. Cell proliferation by MTT assay

Cell viability was determined by the MTT assay, using primary fibroblasts isolated from tissue extracted from Balb/c mice after enzymatic digestion with collagenase (Research Ethics Committee

approval number: CEI-2025-1-31). The cells were maintained in DMEM culture medium (with 10% bovine fetal serum and 2% antibiotic) and then seeded (5000 cells per well) using two 96-well culture plates (each to measure cell viability at 24 and 48 h), repeated in triplicate. Cells were exposed to the textile Ag/PVP samples; the textile was cut to insert them into the wells and, prior to the assay, textile samples were washed with ethanol and allowed to air dry inside a working hood for a sterile environment. Two controls were included: cells only and cells exposed to virgin textile (cotton gauze, Curapack). Plates were incubated for 24 and 48 h at 37 °C (5% CO_2, humidified environment). After each incubation time, the culture medium was removed from each well, washed with PBS, replenished with a solution of 150 µL of new culture medium and 50 µL of MTT solution (5 mg/mL, using sterile PBS as solvent), and left in the incubator for one additional hour. Subsequently, the formazan crystals formed were solubilized in DMSO for absorbance measurement at 570 nm using a microplate spectrophotometer (Benchmark Plus, Bio-Rad). The percent cell viability was calculated using Eq 4:

$$\text{Cell viability (\%)} = \frac{\text{Absorbance of sample}}{\text{Absorbance of control (cells)}} \times 100\% \quad (4)$$

2.9. Evaluation of Ag/PVP nanoparticle release in simulated biological fluid

For this test, 0.35 g of the textile Ag/PVP (corresponding to half a textile) was placed in a 50 mL capacity beaker, and 25 mL of simulated body fluid (SBF) was added at 37 °C. Previously, both the beakers and the SBF (simulated biological fluid) had been preheated at 37 °C. SBF was prepared according to the protocol established by Kokubo and Takadama [47]. The beakers were covered with plastic film to prevent evaporation and kept at 37 °C in the dark and in static conditions. Subsequently, after 1, 3, 6, 12, 24, and 48 h, the textile was removed with tweezers, and the absorbance of the liquid was immediately analyzed in the UV-Vis region (at 400 nm), using SBF as a blank solution. For each sampling time, three replicates of each type of textile were analyzed. To quantify the nanoparticles released into the medium, a calibration curve was constructed with the colloidal solution of Ag/PVP nanoparticles (synthesis: sample 1 US) at 8 different concentrations (in triplicate), in the range of 0.08–31.75 µg Ag/mL (concentrations were stoichiometrically calculated assuming a complete reduction of Ag^+ from $AgNO_3$, which would be part of the Ag/PVP nanoparticles, giving a plasmonic signal at 400 nm), achieving excellent linearity ($R^2 = 0.989$). The limit of detection (LOD) and limit of quantification (LOQ) were determined according to a signal:noise ratio of 3:1 and 10:1, respectively, from the standard deviation of the blank (SBF, n = 3) and the slope of the calibration curve. The LOD and LOQ obtained were 0.175 and 0.582 µg/mL (equivalent to 0.072 and 0.093 absorbance units).

2.10. Statistical analysis

The data obtained were subjected to an analysis of variance (ANOVA) and a Tukey post-hoc test, with a statistical significance value of $p < 0.05$.

3. Results and discussion

3.1. Morphological analysis based on impregnation time and ultrasound-assisted dispersion

Figure 1 shows the different scanning electron microscopy (SEM) images of the textiles obtained, also showing the virgin textile and the activated textile. Figure 1 shows that in the activated textile sample (Figure 1b), fibers are swollen compared to the virgin sample (Figure 1a). In the higher-magnification SEM image (Figure 1g), the average particle size of sample 1 is 20.7 ± 8.9 nm (Figure 2); although it shows dispersion of the particles on the fiber, agglomerates >40–70 nm are also found. In sample 1 + 24 h of impregnation, the number of nanoparticles on the substrate increased (Figure 1h); higher-magnification images show an average particle size of 28.17 ± 5.5 nm (Figure 2). For sample 1 ultrasound (1 US), obtained after 30 min of ultrasound (Figure 1i), a greater deposition of nanoparticles on the fibers was observed, resulting in an average particle size of 19.98 ± 4.3 nm (Figure 2). For the sample obtained after ultrasound and 24 h in impregnation (Figure 1j), an average size of 20.3 ± 10.1 nm was found (Figure 2), presenting a greater amount of agglomerates (>60 nm) than in the textile obtained after ultrasound for 30 min. The textile impregnated for 30 min of reaction in an ultrasonic bath revealed better dispersion of particles on the substrate and a smaller average particle size.

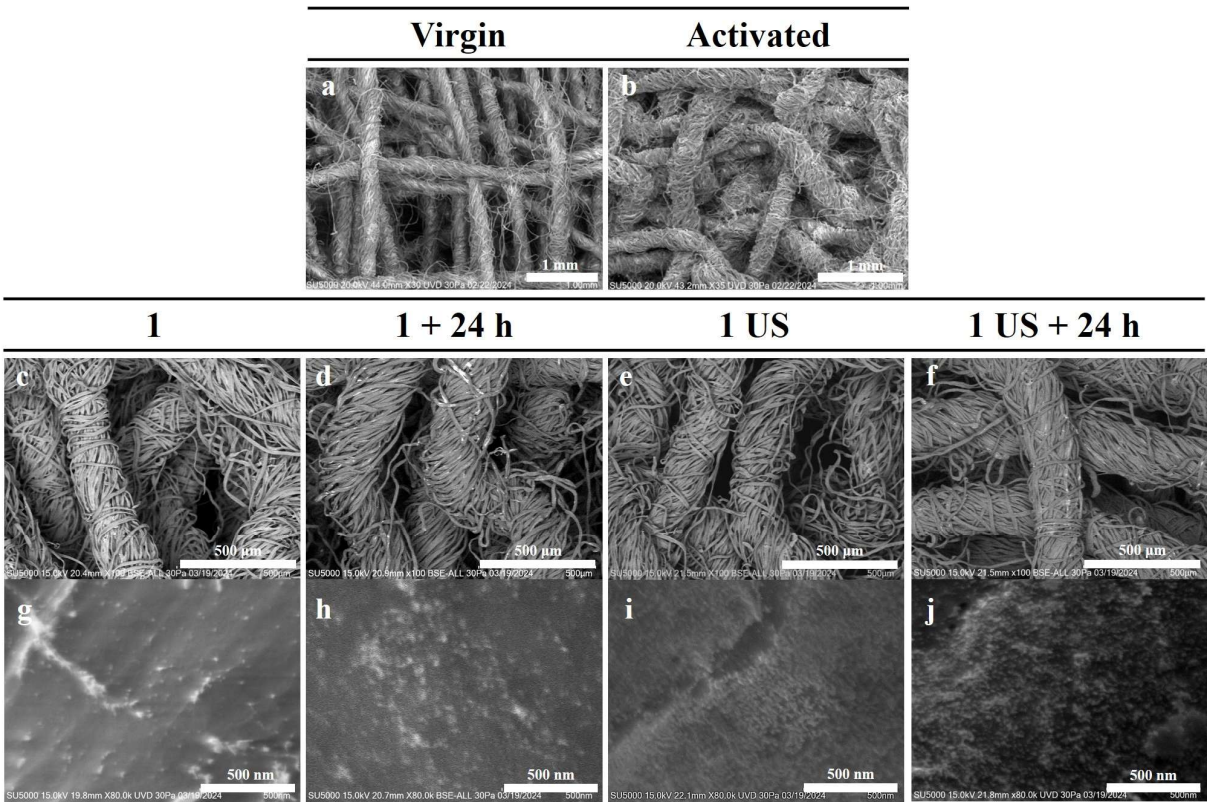

Figure 1. SEM images: virgin, activated, sample 1, sample 1 + 24 h, sample 1 US, and sample 1 US + 24 h.

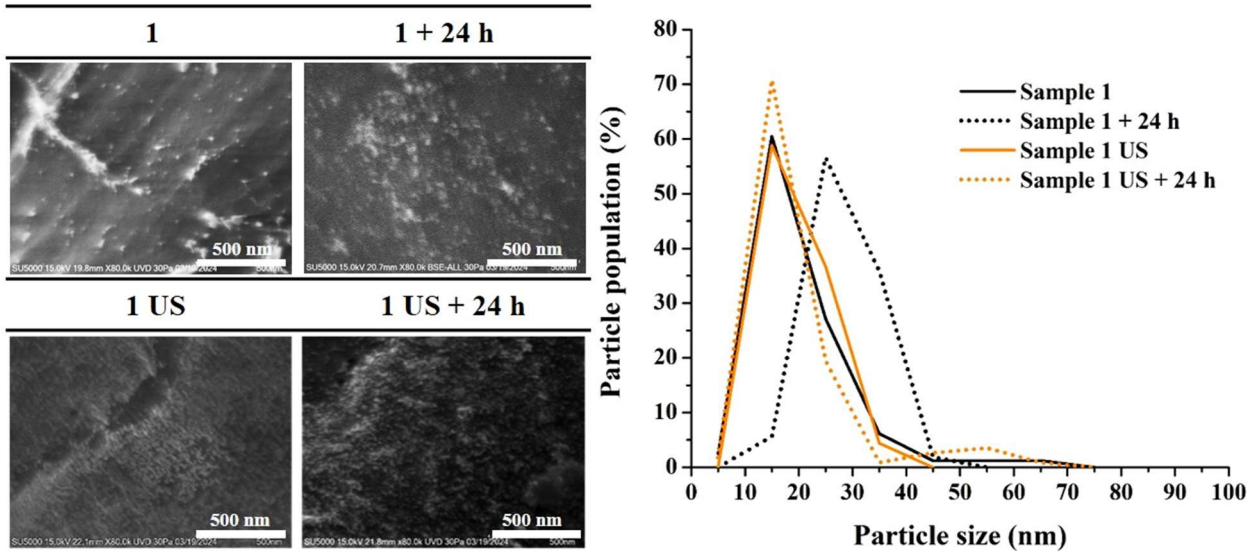

Figure 2. SEM images and particle size analysis, presented as percentage of particles from SEM images (from sample 1: 85 particles; from sample 1 + 24 h: 153 particles; from sample 1 US: 168 particles; from sample 1 US + 24 h: 113 particles).

3.2. Experimental design of the alkalinity of the activated textile

The absorbance spectra of the reaction solutions (Table 2) are shown in Figure 3, together with a table summarizing the pH evolution during synthesis. For the impregnation, two textiles were used, synthesized at pH 7.2, 9.3, and 11.5, at a reaction temperature of 26 °C. The absorbance spectra of the reaction solutions prepared without textiles at 18 and 30 °C are also shown, in order to observe the influence of temperature on the synthesis and to compare it with syntheses involving the impregnation of alkaline (pH 9.3 and 11.5) and neutral (pH 7.2) textiles.

Comparing the spectra of the reactions without textiles (black dotted lines), it is observed that the temperature does not have a significant effect on the synthesis, since the absorption bands are similar. The spectrum obtained at room temperature is slightly more symmetrical, although both conditions show the same absorbance value at 400 nm (1.22 Abs U.) and the same onset of absorption. In addition, the curves without textile exhibit a higher plasmonic signal (~400 nm) than those prepared in the presence of textile. This indicates that, in the presence of textile, fewer free nanoparticles remain in suspension. This can be attributed to the textile acting as a substrate for Ag^+ adsorption, enabling nucleation on the fiber surface. Consequently, less Ag^+ remains in solution to form free Ag/PVP nanoparticles, indicating a transfer of Ag to the textile [48–50].

The reaction solutions in which textiles were impregnated show absorption onsets at longer wavelengths, namely 575, 676, and 687 nm for pH 7.2, 9.3, and 11.5, respectively. In addition to the characteristic silver plasmon absorption band at 390–394 nm, the solutions with textiles at pH 7.2 exhibit absorption edges at 467 and 526 nm. For the gauze solutions at pH 9.3 and 11.5, three additional edges are revealed at 590, 637, and 667 nm, indicating the presence of larger particles in solution.

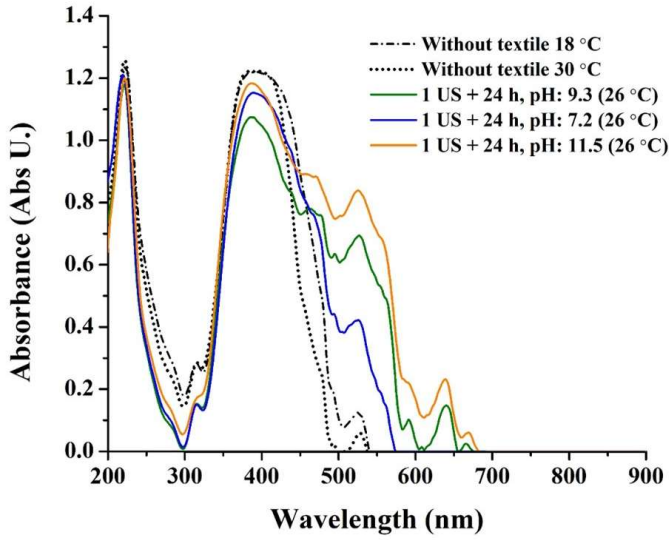

Synthesis stage	Solution pH: 1 US + 24 h at pH 9.3	Solution pH: 1 US + 24 h at pH 7.2	Solution pH: 1 US + 24 h at pH 11.5
Water-PVP-$AgNO_3$	4.2	4.2	4.2
Water-PVP-$AgNO_3$ + activated textiles	4.6	4.5	5.6
End of reduction	7.7	7.4	7.7

Figure 3. Absorbance spectra of 5% reaction solutions in distilled water and results of pH monitoring at each stage of the synthesis. Photographs of the 5% reaction solutions in distilled water (the same solutions analyzed to obtain absorbance spectra) are shown.

Figure 4 shows SEM images of the textiles and the results of particle size measurement (two images per textile) adsorbed on the different textiles obtained under the synthesis of sample 1 US (absorbance in Figure 3), after 24 h of impregnation in reaction solutions using textiles with different pH values (9.3, 7.2, and 11.5). Comparing the SEM images of the textiles, a higher concentration of nanoparticles is observed for the textile with pH 7.2, with an average size of 28.8 ± 14 nm, with approximately 50% of the particles in the 20–30 nm size range. For the textile at pH 9.3, an average particle size of 35.9 ± 24.2 nm is observed, with ~40% of particles in the 20–30 nm size range. For the textile with higher alkalinity (pH 11.5), an average size of 36.1 ± 18.5 nm was found, with ~40% of particles also in the 20–30 nm range.

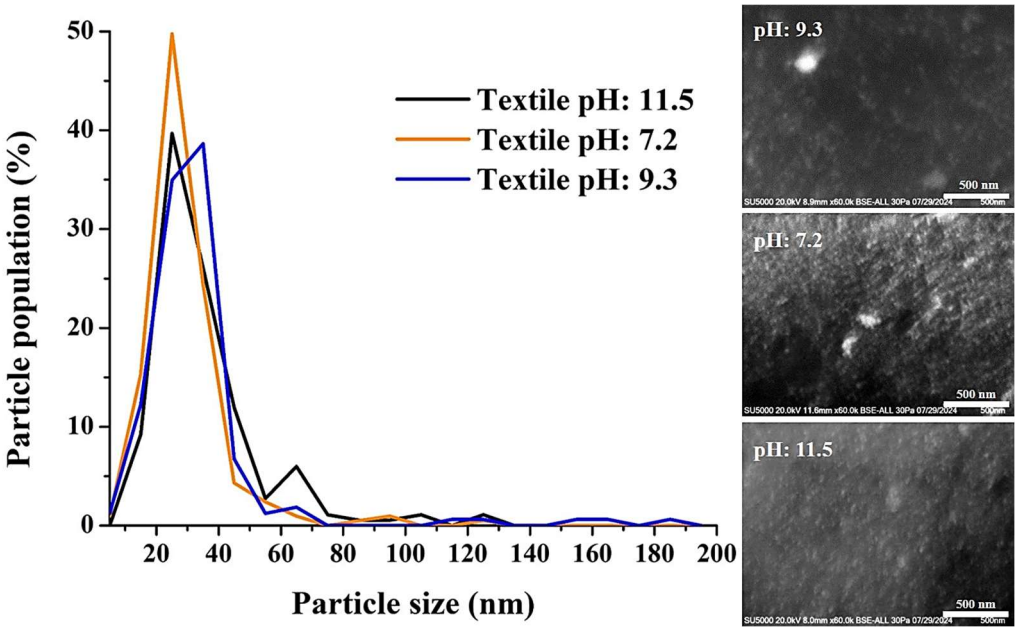

Figure 4. SEM images of textiles made using activated textiles at different pH values (synthesis sample 1 US left for 24 h of impregnation) and particle size analysis, presented as percentage of particles (from SEM images, two images analyzed by sample type: from textile pH 9.3, 163 particles; from textile pH 7.2, 209 particles; from textile pH 11.5, 184 particles).

3.3. Water absorption capacity

Figure 5a shows the water retention capacity of the textiles. The activated textile showed a decrease of approximately 6% with respect to the virgin textile (649% ± 44%), although this difference was not statistically significant (ANOVA). Sample 1 decreased ~3.4% relative to the activated textile (also not statistically significant). Although an increase in absorption was expected due to the presence of the hygroscopic PVP polymer coating the metal nanoparticles, the decrease in water absorption capacity may be attributed to the reduction of the space between the cellulosic fibers due to swelling from the alkaline treatment, as observed in the SEM images (Figure 1b), in addition to a possible hydrophobic effect of silver.

The largest decrease was recorded in sample 1 with 24 h of impregnation (~8.5% with respect to the activated textile), coinciding with a higher loading of nanoparticles on the substrate (SEM images in Figure 2). This is the only sample showing a statistically significant difference with respect to the virgin textile ($p = 0.006$). For the textiles obtained by the ultrasonic method, no significant differences are observed with respect to the activated textile, indicating that ultrasonic dispersion does not significantly affect the water absorption capacity of the textiles.

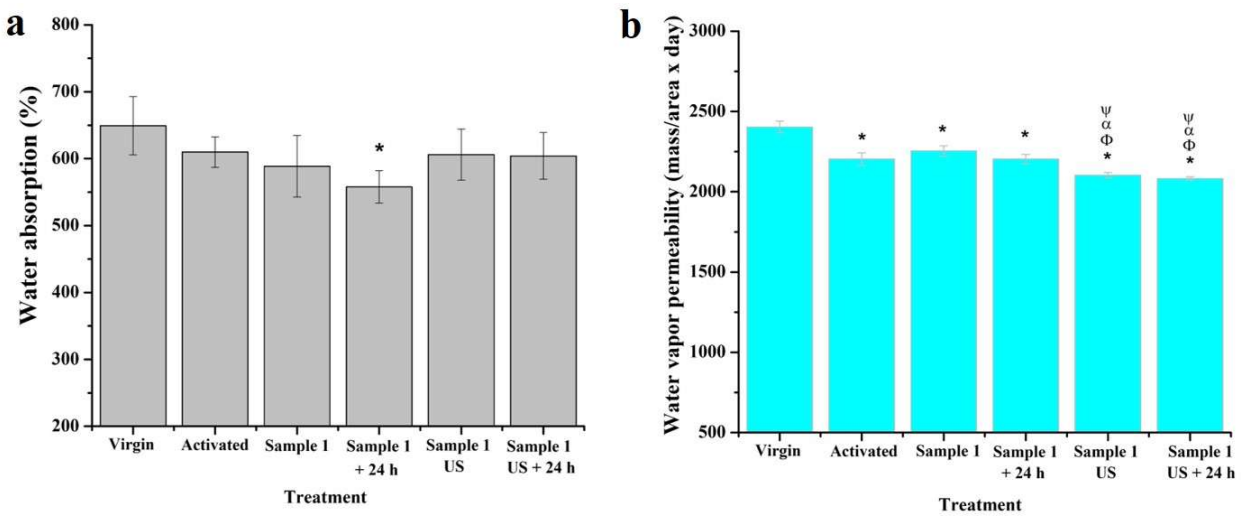

Figure 5. a: Water absorption capacity, expressed as the mean ± standard deviation (n = 5). Statistical comparison among the six groups of samples ($p < 0.05$): *: significant difference vs. virgin textile. b: Water vapor permeability, expressed as mean ± standard deviation (n = 3). Statistical comparison among the six groups of samples ($p < 0.05$): *: significant difference vs. virgin; Φ: significant difference vs. activated textile; α: significant difference vs. sample 1; ψ: significant difference vs. sample 1 + 24 h.

3.4. Water vapor permeability

Figure 5b shows the results of water vapor permeability of the textile. This test evaluates breathability, i.e., the capacity to allow water vapor to pass through the textile (24 h at 37 °C). The virgin textile presents high permeability, which is desirable for adequate gas exchange [32]. The results show that the activated textile reduced its permeability by 8.3% with respect to the virgin textile, due to the closure of spaces between the fibers after the alkaline treatment, with statistical significance ($p = 0.00003$). Sample 1 had 2.29% higher permeability than the activated textile, possibly due to the magnetic agitation during the metallic reduction that causes the fibers to loosen and the weft to open, although without statistical significance. Sample 1 with an additional 24 h of impregnation showed similar permeability to the activated textile, although slightly lower than sample 1 (2.2% lower), without statistical significance.

On the other hand, textiles prepared using ultrasonic treatment show the lowest permeability compared with the activated textile, with sample 1 US and sample 1 US + 24 h showing decreases of 4.5% and 5.5%, respectively. Both showed statistical significance relative to the activated textile, but not between each other. They also differ significantly from samples without ultrasound (under magnetic agitation). Overall, alkaline treatment has the greatest impact on reducing water vapor permeability. However, ultrasonic treatment further enhances this reduction, suggesting that adsorption of the Ag/PVP nanoparticles intensifies this effect. One possible contribution is the increased presence of nanoparticles on the fibers, with the PVP polymer acting as a moisture absorber.

3.5. Mechanical properties

The results of elongation (%) and breaking strength (MPa) are shown in Figure 6. An increase in elongation is observed in all samples (Figure 6a) with respect to the virgin textile (10.27%). The values for the activated textile, sample 1, sample 1 + 24 h, sample 1 US, and sample 1 US + 24 h were 38.94%, 48.41%, 40.91%, 35.74%, and 40.91%, respectively. This elastic behavior is already observed in the activated textile sample, as alkaline treatment causes fiber swelling, as seen visually and in SEM micrographs (Figure 1b), resulting in shortening of the textile fibers. This shortening allows greater extension compared to the virgin textile, which appears flatter and with a more open weft. The highest elongation relative to the activated textile was observed in sample 1, being the only treatment with statistical significance (p = 0.02). For sample 1 with ultrasound treatment, the percentage of elongation decreased with respect to the activated textile and sample 1, with statistical significance found only with respect to the latter (p = 0.0016). The textiles obtained by impregnation for 24 h presented the same percentage of elongation, and no statistical significance was found with respect to the activated textile (p = 0.97).

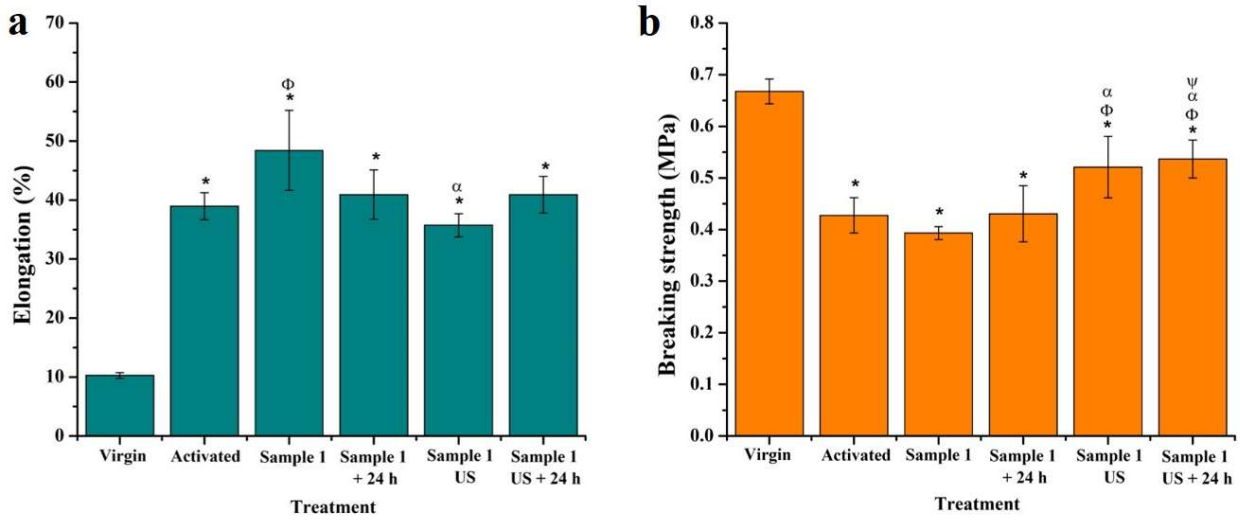

Figure 6. a: Percentage elongation, expressed as mean ± standard deviation (n = 4). Statistical comparison among the six groups of samples ($p < 0.05$): *: significant difference vs. virgin textile; Φ: significant difference vs. activated textile; α: significant difference vs. sample 1. b: Tensile strength of the fabric, expressed as mean ± standard deviation (n = 4). Statistical comparison among the six groups of samples ($p < 0.05$): *: significant difference vs. virgin; Φ: significant difference vs. activated textile; α: significant difference vs. sample 1; ψ: significant difference vs. sample 1 + 24 h.

As for the breaking strength (Figure 6b), the virgin textile had the highest value (0.668 MPa). All treated samples showed lower values. The activated textile presented 36% less resistance, and sample 1 presented the lowest resistance of all samples (0.393 MPa), although it did not present statistical significance with respect to the activated textile. Sample 1 with 24 h of impregnation (sample 1 + 24 h) presented the same decrease in resistance as the activated textile, with no statistically significant differences relative to sample 1. Textiles obtained by ultrasound treatment preserved better resistance (0.521 and 0.537 MPa for sample 1 US and sample 1 US + 24 h, respectively). Statistical

significance was found with respect to the activated textile ($p = 0.041$ and $p = 0.013$). In addition, there were significant differences between sample 1 and those treated with ultrasound ($p = 0.0033$ and $p = 0.001$). In this case, the alkaline treatment was the precursor of the decrease in tensile strength, as the introduction of –OH species in the alkaline solution weakens the interfibrillar bonds given by hydrogen bridges between cellulose chains. Although rinsing/neutralization was expected to limit this effect, this was not observed. The use of ultrasound, however, resulted in increased breaking strength compared to the activated textile (~22% for sample 1 US and 25% for Sample 1 US + 24 h). This can be attributed to the fact that ultrasound enhances the diffusion and incorporation of the Ag/PVP nanoparticles into the fibers, strengthening them [33,35].

3.6. Infrared analysis by FTIR

Figure 7a shows the infrared spectra (FTIR) obtained from the samples of virgin textile, activated textile, and sample 1 US + 24 h of impregnation. No apparent changes with respect to the virgin textile are observed by the naked eye. Regarding the structure of cellulose forming the cotton, the peaks at 3300 and 3282 cm^{-1} correspond to the stretching of the hydroxyl groups (–OH) of the intra- and intermolecular hydrogen bonds, respectively [51,52]. The vibration at 2892 and 2860 cm^{-1} corresponds to the asymmetric and symmetric stretching of the $–CH_2–$ bond, respectively. The broad band at 1650 cm^{-1} is associated with the H–O–H stretching vibration of water adsorbed to the fibers [53]. The peak at 1425 cm^{-1} corresponds to the scissoring of the CH_2 bond. The peak at 1314 cm^{-1} corresponds to the rocking bending of the C–H bond. At 1204 cm^{-1}, C–O stretching is observed. A sharp peak at 1159 cm^{-1} is associated with stretching of the anti-symmetric C–O–C bridge [51,53]. At 1106 cm^{-1}, an anti-symmetric ring stretching vibration is observed [51,54]. The peaks at 1055 and 1027 cm^{-1} are associated with C–O and C–C bond stretching vibrations, respectively [53]. The frequency at 893 cm^{-1} is attributed to the bond between two glucose units (β-bond) forming cellulose [53]. At 664 cm^{-1}, there is out-of-plane bending of the OH bond [51]. Due to the amount of polymer used in synthesis (0.8% by weight with respect to the reaction solvent), it is not possible to observe the most intense peaks of the PVP polymer, which would appear at 1652 cm^{-1} due to the stretching vibration of the C=O carbonyl group, at 1420 cm^{-1} reflecting the –N–C– bond, and at 1280 cm^{-1} from the stretching vibration of the C–N bond [55,56].

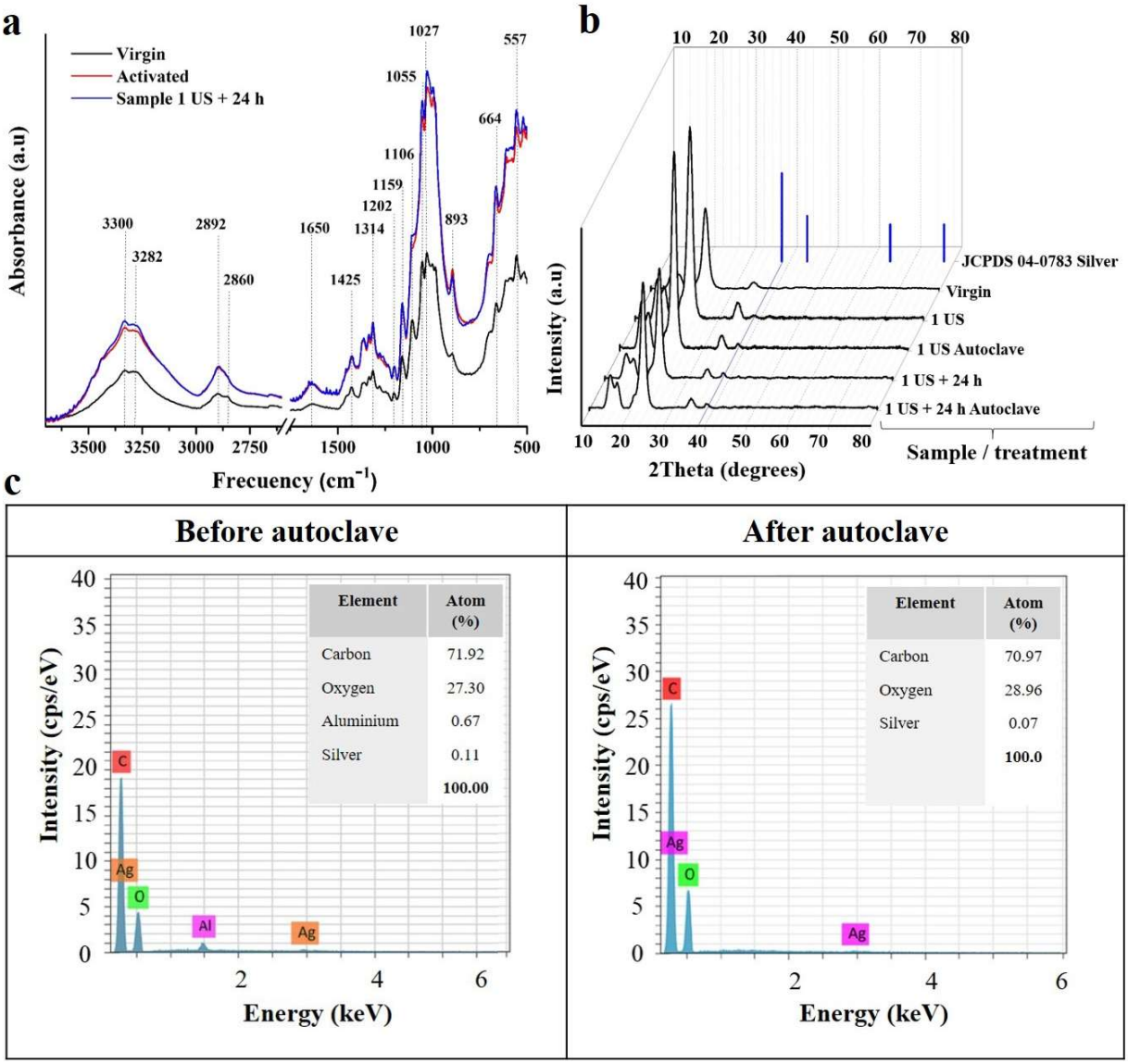

Figure 7. a: IR spectra of textiles (region 2600–1730 cm^{-1} is omitted). b: Diffractograms of the textiles: virgin textile, original textile Ag/PVP (sample 1 US and sample 1 US + 24 h), and after autoclave sterilization (silver diffraction pattern JCPDS 04-0783 is shown in blue). c: EDX analysis (sample 1 US + 24 h) before and after autoclaving.

3.7. XRD analysis of original vs. autoclaved textiles

Figure 7b shows the diffractograms obtained from the original samples and post-sterilization textiles, including the virgin gauze. The diffractogram of the untreated gauze shows characteristic peaks of cellulose I at 2θ = 15.4°, 17.1°, 23.4°, and 35.1° [57,58]. In the diffractogram of sample 1 ultrasound and sample 1 ultrasound + 24 h of impregnation, both before and after sterilization, another peak appeared at 38.6°, attributed to the (111) plane of silver (FCC), according to diffraction pattern JCPDS No. 04-0783 [59], which corresponds to the most intense crystallographic reflection. Complementary EDX analysis was performed on both the non-autoclaved sample (sample 1 US + 24 h) and the autoclaved sample (Figure 7c). In both cases, the spectra exhibited the main expected elements, especially C, O, and Ag, confirming that silver remained detectable after sterilization. Semi-quantitative

analysis based on atomic percentages showed only slight variations between the samples. The relative Ag content decreased from 0.11 to 0.07 atomic%, whereas the C and O contents remained within similar ranges, suggesting that autoclaving did not produce major qualitative changes in the surface elemental profile. A minor Al signal was also detected, likely originating from the aluminum SEM sample holder.

3.8. Morphology of original vs. autoclaved textiles

Particle size was determined from SEM images of textiles subjected to wet sterilization (autoclaved at 121 °C at 15 psi for 35 min and then heat dried at 120 °C for 45 min), in order to compare with the original textiles of sample 1 US and sample 1 US + 24 h impregnation (Figure 8). In sample 1 US, the autoclaved sample shows larger particles compared to the original. Approximately 57% of the particles are in the 20–30 nm range (average size 28.41 ± 7.12 nm), whereas in the original sample, ~59% of the particles are between 10 and 20 nm (average size 19.98 ± 4.31 nm). For sample 1 US + 24 h, an increase in particle size compared to the original sample was also found: after autoclaving, ~55% of the particles were between 20 and 30 nm (average size 28.41 ± 10.41 nm), while for the original sample of the same type, ~71% of the particles corresponded to the 10–20 nm (average size of 20.3 ± 10.1 nm). The two autoclave-treated samples presented equal average size; however, sample 1 US + 24 h presented greater particle size dispersion (standard deviation of 10.1 nm in sample 1 US + 24 h vs. 7.12 nm in sample 1 US) and ~4% of particles in the 55–90 nm range, which are not observed in sample 1 US.

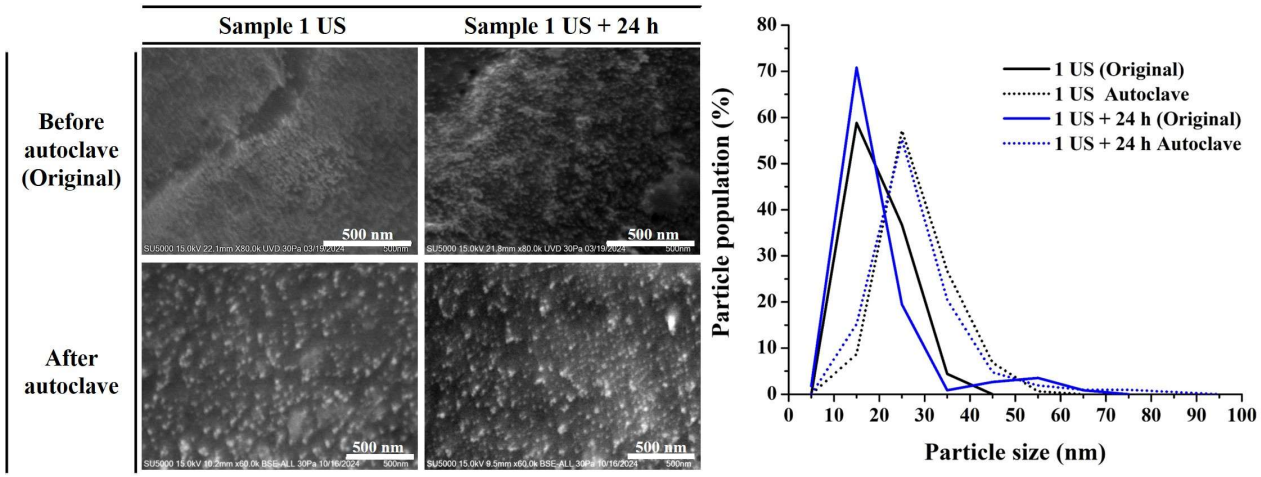

Figure 8. SEM images and particle size analysis of original textiles and after autoclave sterilization, presented as percentage particle population from SEM images (from sample 1 US: 168 particles; from sample 1 US + 24 h: 113 particles; from sample 1 US autoclave: 161 particles; from sample 1 US + 24 h autoclave: 210 particles).

The humid environment, combined with the pressure, caused a rearrangement of the nanoparticles, leading to more individualized and clearly distinguishable particles with spherical morphology and better dispersion on the fiber surface. Although sterilization at 121 °C is well below the glass transition temperature (T_g) of PVP (Mw 40 k, ~160–170 °C under dry conditions) [60], its hygroscopic nature

allows water vapor to reduce the effective T_g. In this new hydrated state, PVP exhibits increased molecular mobility, facilitating reorganization on the substrate. This moisture-induced plasticization effect has been previously reported [61–63].

3.9. Evaluation of antimicrobial capacity of original vs. autoclaved textiles

The samples evaluated for antimicrobial evaluation, under ASTM E-2149 (with modifications) [64–67] were those prepared by ultrasonic dispersion (sample 1 US and sample 1 US + 24 h). Additionally, to observe the post-sterilization antimicrobial behavior, the samples were autoclaved. The control samples were sterile virgin gauze. The bactericidal effect was evaluated by the reduction in colony formation compared to the control sample (sterile virgin gauze). For *Staphylococcus aureus*, decreases of 94.75% ± 0.68% and 94.67% ± 0.39% were observed for sample 1 US and sample 1 US + 24 h. On the other hand, decreases of 94.47% ± 0.44% and 95.56% ± 0.87% were observed for the sample 1 US autoclave and sample 1 US + 24 h autoclave, respectively. In contrast, the bactericidal effect against *Escherichia coli* was higher, resulting in decreases of 99.1% ± 0.973% and 99.57% ± 0.19% sample 1 US and sample 1 US + 24 h, as well as 98.84% ± 1.5% and 98.9% ± 0.08% for the sample 1 US autoclave and sample 1 US + 24 h autoclave, respectively. The analysis of variance showed no significant differences between samples for the same bacteria.

Although autoclave sterilization increased the average nanoparticle size, this change did not result in a statistically significant reduction in antibacterial performance. For sample 1 US, the average particle size increased from 19.98 ± 4.31 to 28.41 ± 7.12 nm after sterilization, corresponding to an increase of approximately 42.2%. Likewise, for sample 1 US + 24 h, the average size increased from 20.3 ± 10.1 to 28.41 ± 10.41 nm, corresponding to an increase of approximately 40.0%. In both cases, the particle size distribution shifted from mainly 10–20 nm in the original textiles to mainly 20–30 nm after sterilization. A possible explanation is that, despite this increase, the nanoparticles remained within a size range still compatible with effective antibacterial action. Moreover, the retained presence of Ag on the fibers and the continued release of silver species may have contributed to preserving the antibacterial response after autoclaving. Figure 9 shows the plate cultures at 24 h of incubation.

The antibacterial activity of Ag/PVP nanoparticles has been extensively studied, being effective for both gram-positive and gram-negative bacteria, hence the inclusion of Staphylococcus aureus (+) and Escherichia coli (–) in this study [30,68]. The differences in response against S. aureus and E. coli (higher percentages for E. coli) are consistent with the literature: it has been reported that silver nanostructures show higher effectiveness against gram-negative bacteria. Due to the structure of the cell envelope, gram-negative cells have a thinner peptidoglycan layer and a membrane rich in lipopolysaccharides, which facilitates the interaction of nanoparticles and Ag^+ ions with the membrane. On the other hand, gram-positive cells have a thicker peptidoglycan layer acting as a partial barrier to diffusion [68–70].

Moreover, intimate contact between Ag nanoparticles and the bacterial surface has been reported to enhance silver uptake and, consequently, to increase toxicity, highlighting the importance of achieving a good dispersion of silver NPs on the textile substrate and their stabilization with polymers such as PVP [71,72].

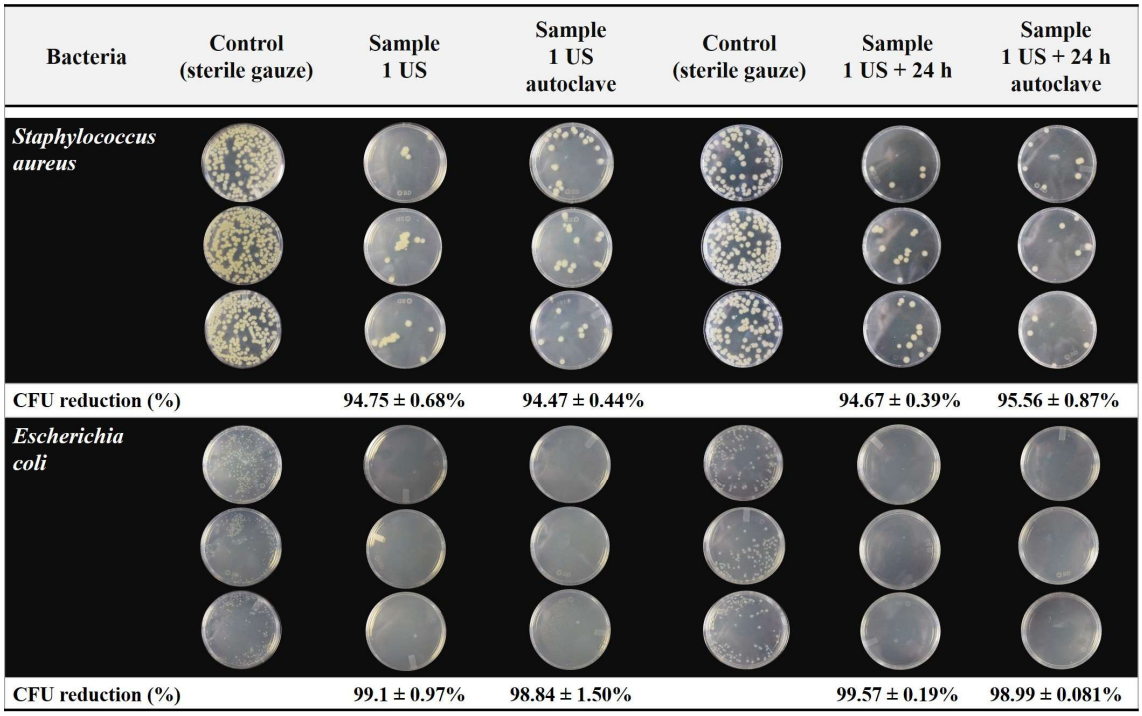

Figure 9. Bactericidal effect of original textile samples treated with ultrasound (sample 1 US) and ultrasound + 24 h of impregnation (1 US + 24 h), and samples post-sterilization by autoclave on *Staphylococcus aureus* and *Escherichia coli* bacteria, under ASTM E-2149. Percentage CFU (colony forming units) reduction expressed as mean ± standard deviation (n = 3). Shown are culture plates at the same prepared dilution.

In addition, size is a critical factor in the antibacterial action of silver nanoparticles, as it will determine how the bacterial cell membrane responds. For example, it has been found that a smaller particle size (<10–20 nm) represents a larger specific area, releasing more metal ions, which can penetrate and adhere to the cell membrane, more quickly altering its function. A greater release of metal ions has been associated with the generation of reactive oxygen species that induce oxidative stress [73–76].

In this context, the PVP used, with an average molecular weight of 40 k, provided good stability to the system, preventing the formation of larger particles on the cellulose fibers and favoring the permanence of nanoparticles in the range of 20–30 nm for sterilized textiles. Although no direct evidence of PVP layer thickness after sterilization was obtained, the preserved antibacterial activity and release behavior suggest that the coating did not undergo changes severe enough to fully hinder silver-species release [70].

Although there are studies reporting adequate stability against multiple washing cycles in cellulosic textiles functionalized with PVP-stabilized silver nanoparticles [77,78], as well as in synthetic substrates such as nylon 6,6 [79,80], studies explicitly evaluating post-autoclave sterilization antibacterial performance in cotton-Ag/PVP systems remain scarce. To date, no direct pre-autoclave vs. post-autoclave analysis has been reported in textile Ag/PVP. The closest evidence comes from two complementary lines of research. The first applied an autoclave cycle at 121 °C for 15 min as the thermal process to form metallic silver directly on cotton cellulose fibers and reported significant

antibacterial activity, which suggests that the nanoparticles on the fibers can withstand autoclave conditions without losing functionality [81]. The second investigated the impact of the autoclave process on the antibacterial capacity of Ag NPs adsorbed on PVA (polyvinyl alcohol) fibers, reporting a loss in antibacterial activity, attributed to an increase of ~247% in the size of the nanoparticles [44,82].

3.10. Evaluation of Ag/PVP nanoparticle release in a simulated biological fluid

The homogeneity of the impregnation was evaluated by comparing the coefficient of variation (CV, %), also called relative standard deviation [83], between the textiles impregnated by ultrasound (sample 1 US and sample 1 US + 24 h), using the absorbance at 400 nm as the signal associated with the presence of Ag/PVP nanoparticles released into the simulated biological fluid (SBF) under static conditions.

The absorbance results of plasmonic silver release from textiles (sample 1 US and sample 1 US + 24 h) in SBF solution at different times (1, 3, 6, 12, 24, and 48 h) are shown in Figure 10a reporting the comparison of the homogeneity of impregnation with the coefficient of variation (%). For the sample 1 US (30 min of impregnation in ultrasonic bath), from the first to the third hour, the coefficients of variation were high (1 h, 33.1%; 3 h, 47.6%), indicating a very variable release between samples or low homogeneity in the impregnation. At longer times, the CV value decreased (6 h, 15.4%; 12 h, 18.7%), indicating a higher homogeneity of the nanoparticles on the cellulosic substrate. However, at 24 h, it had the highest CV (55.8%), which stabilized for 48 h (5.9%).

In contrast, the sample 1 US + 24 h (with an additional 24 h of static impregnation) showed initial absorbance below LOQ but reached quantifiable values with consistently low CV (between 6.9% and 10.7%) from 3 h onward, reflecting a more uniform and controlled release. These results suggest that an additional 24 h of static impregnation improves the uniformity of impregnation on the substrate. Moreover, the more controlled release profile observed for sample 1 US + 24 h indicates a more stable loading on the gauze surface, with a lower tendency to rapid shedding under the evaluated conditions.

Figure 10b shows the release of Ag/PVP nanoparticles (μg/mL) for the two types of textiles, using the equation $A = 0.0517C + 0.0635$ (Figure 10c). In both groups, a progressive increase in the release of Ag/PVP nanoparticles was observed with time. However, the magnitude and kinetics of release differed markedly between textiles. Sample 1 US (only allowed to impregnate during the 30 min reduction time in ultrasonic bath) showed an initial release detected from the first hour (~1.0 μg/mL), exceeding the method's limit of quantification (LOQ = 0.582 μg/mL). The concentration then increased steadily to reach values of ~5.1 μg/mL at 48 h. This behavior suggests an initial rapid release phase followed by a more sustained release stage, possibly associated with the gradual diffusion of nanoparticles retained in the cellulosic fibers. In contrast, sample 1 US + 24 h (textile with an additional 24 h of static impregnation after ultrasound) presented an initial release of almost zero at the first hour (below the LOD = 0.175 μg/mL), followed by a gradual increase from 3 h onward. Concentrations reached a maximum of 2.1 μg/mL at 24 h, with no significant subsequent increases (no statistical significance between times 24 and 48 h). This behavior indicates that the 24 h impregnation after reduction in the ultrasonic bath helped to form a more stable surface layer, where the additional time allowed greater coverage of Ag/PVP nanoparticles on the fibers, favoring greater interaction as hydrogen bridges between the carbonyl group C=O of the PVP and the O–H group of the cellulose polymeric chains, thus reducing the release rate of the nanoparticles to the medium [84]. Importantly, the 48 h release period used in this study is consistent with clinical practice: infection-prevention

guidelines recommend sterile dressings to remain in place for approximately 24–48 h after surgery, and silver-containing dressings are commonly designed for use over similar time intervals before being changed [85–87].

a

Time (h)	Sample 1 US Absorbance at 400 nm (Mean ± SD)¤	CV* (%)	Sample 1 US + 24 h Absorbance at 400 nm (Mean ± SD)¤	CV* (%)
1 h	0.115 ± 0.04	33.1	0.064 ± 0.02	31.0
3 h	0.126 ± 0.06	47.6	0.093 ± 0.01	10.2
6 h	0.142 ± 0.02	15.4	0.124 ± 0.01	6.9
12 h	0.198 ± 0.04	18.7	0.132 ± 0.01	7.2
24 h	0.199 ± 0.11	55.8	0.168 ± 0.02	10.7
48 h	0.329 ± 0.02	5.9	0.137 ± 0.02	16.0

¤: Three repetitions per time
*: Coefficient of variation (CV = SD/Mean * 100)

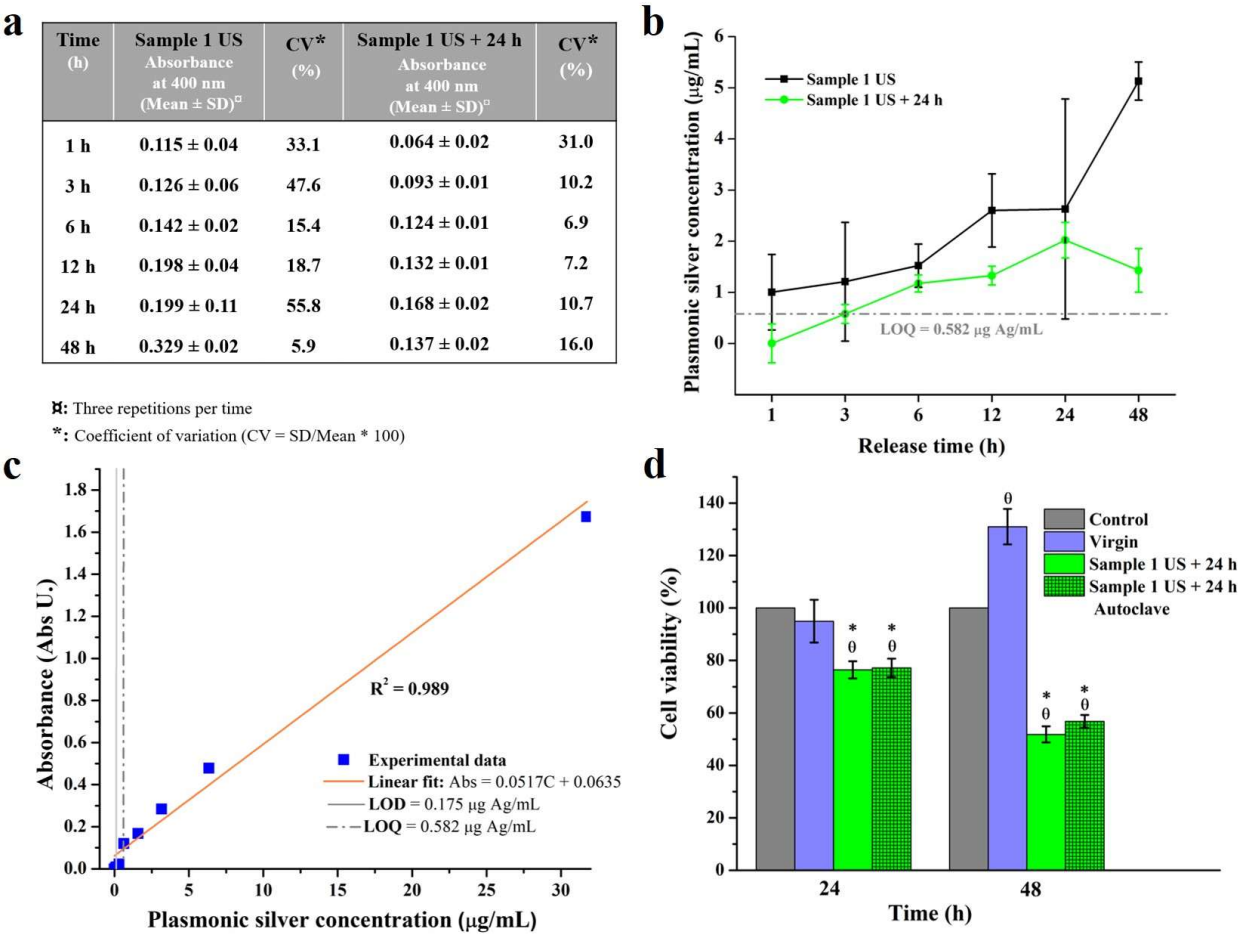

Figure 10. a: UV-Vis absorbance results (at 400 nm) for each release time, expressed as mean ± standard deviation (n = 3), including the coefficient variation (CV = SD/mean × 100). b: Release profile of Ag/PVP nanoparticles for sample 1 US and sample 1 US + 24 h, calculated from absorbance values using the calibration curve equation. Error bars represent the standard deviation. The dashed line indicates the quantification limit (LOQ = 0.582 µg Ag/mL). c: Calibration curve for Ag/PVP nanoparticles obtained by UV-Vis spectroscopy. The plot shows the relationship between absorbance (at 400 nm) and plasmonic silver concentration in the range of 0.08–31.7 µg/mL (concentrations were calculated stoichiometrically assuming complete reduction of Ag^+ from $AgNO_3$, and that it would be part of the Ag/PVP nanoparticles). The linear regression equation was A = 0.0517C + 0.0635 with R^2 = 0.989. The LOD and LOQ were 0.175 µg/mL and 0.582 µg/mL, respectively. d: Graph of cell viability (by MTT assay) at 24 and 48 h. Results are presented as the mean ± standard deviation (n = 3). Comparison was made between four groups and the same time (control, virgin textile, sample 1 US + 24 h, and sample 1 US 2 + 24 h autoclave). Statistical comparisons among the four groups of samples ($p < 0.05$): θ: significant difference vs. control (only cells), *: significant difference vs. virgin.

3.11. Cell proliferation by the MTT assay

The sample with the best impregnation homogeneity (sample 1 US + 24 h) was subjected to the MTT assay to evaluate the proliferation of primary cultured fibroblasts after 24 and 48 h. In addition, the autoclaved sample (sample 1 US + 24 h autoclave) was included to assess the effect of sterilization on cell response. The following controls were used: cells only (no textile) to determine baseline viability, and cells exposed to virgin textile (cotton gauze) to assess the influence of the untreated material. Figure 10d shows the MTT assay results. At 24 h of exposure, both sample 1 US + 24 h and autoclaved sample 1 US + 24 h showed cell viabilities of 76.44% ± 3.30% and 77.20% ± 3.53%, respectively. No statistically significant differences were found between them; however, both samples showed significant differences compared with the control (cells only) and the virgin textile ($p < 0.002$). No significant difference was found between the virgin textile and the control.

These results indicate that, at 24 h, both textiles can be considered non-cytotoxic materials, since they exceed 70% cell viability [76]. The observed drop in viability may be attributed to the release of nanoparticles, as evidenced in the SBF release study for sample 1 US + 24 h at 24 h (which, similar to the MTT assay, was carried out under static incubation conditions). In this context, the release of Ag^+ ions from the nanoparticles is also likely [88].

However, extending the test to 48 h resulted in a decrease in viability to 51.81% ± 3.07% and 56.79% ± 2.46% for sample 1 US + 24 h and the autoclaved sample, respectively. No significant differences were found between them, while both samples differed from the control (only cells) and the virgin textile ($p < 0.00001$).

As no increase in nanoparticles released to the medium was detected in the 24–48 h release study, the toxic effect observed at 48 h of exposure is not explained by higher release but may be associated with a cumulative phenomenon. This decrease in viability is in agreement with previous studies showing that the cytotoxicity of PVP-stabilized nanoparticles increases with exposure time due to intracellular accumulation and release of silver Ag^+ ions, which induce oxidative stress and mitochondrial dysfunction. Research has proven that PVP polymer as a coating on silver nanoparticles does improve the stability of the colloid but does not slow down the transformation of metallic silver to ionic silver once the nanoparticles have been internalized into the cells, which causes the cumulative cellular damage observed at prolonged exposure times [88–90].

At 48 h of exposure, the virgin textile (cotton gauze) showed significantly increased cell proliferation to 131.7% ± 6.75%, with a significant statistical difference compared with the control ($p < 0.0001$). This behavior in the virgin textile sample at a longer exposure time may be attributed to the characteristics of cotton, together with the design of the gauze, which is a non-woven textile, whose fibrous and highly porous structure acts as a scaffold that increases cell contact surface area, enhancing cell adhesion and growth [91,92]. Previous studies have shown that cellulose-derived materials, including cotton textiles, can enhance cell proliferation due to their three-dimensional topography and high contact surface [93,94]. In addition, the virgin textile presented the highest values of water absorption capacity and permeability (Figure 5), which generates a more hydrated microenvironment with greater nutrient exchange, conditions that favor cell proliferation [95,96].

From a clinical standpoint, these findings suggest that the current material formulation is more appropriate for short-term wound contact than for prolonged continuous exposure under static in vitro conditions. Although both the non-autoclaved and autoclaved samples maintained cell viability above the commonly accepted non-cytotoxic threshold at 24 h, the reduction observed at 48 h indicates a

time-dependent cytotoxic response that should be considered when defining the intended duration of use. This behavior is likely associated with cumulative exposure to released silver species and/or progressive nanoparticle internalization, rather than with a sudden increase in nanoparticle release after 24 h. Therefore, further optimization should aim to reduce cumulative toxicity by adjusting silver loading, improving release control, and refining coating stability while maintaining antibacterial performance.

4. Conclusions

Gauze impregnated with Ag/PVP nanoparticles was evaluated. The ultrasound-assisted impregnation achieved the best dispersion and particle size. The reaction temperature did not significantly affect the synthesis of the nanoparticles; on the other hand, the alkalinity of the activated textiles favored the formation of larger particles and decreased the density of the nanoparticles on the substrate, while the neutral pH presented the best dispersion and highest particle concentration. The alkaline treatment was the dominant factor in the reduction of water vapor permeability and absorption capacity, while the use of ultrasound partially intensified this effect, maintaining stable water absorption capacity. As for the mechanical performance, the ultrasound-assisted impregnation favored a better incorporation of the nanoparticles into the fibers, strengthening the textile.

The sterilization process modified the average particle size and polydispersity, without affecting the antimicrobial property, showing bacterial colony reductions of approximately 95% for gram-positive *Staphylococcus aureus* bacteria and an effectiveness of more than 99% for gram-negative *Escherichia coli*, without significant changes in the textiles with an additional 24 h of impregnation.

The SBF release study showed that the additional 24 h static impregnation time decisively influences the homogeneity and release kinetics of the Ag/PVP nanoparticles from the textile; the additional 24 h of static impregnation resulted in a more controlled and reproducible release, with low coefficients of variation and with concentrations reaching an equilibrium state before 48 h. In accordance with this trend, the MTT assay showed that samples with 24 h of additional impregnation and the sterilized sample maintained cell viability above the non-cytotoxic threshold at 24 h, while a decrease was observed at 48 h, attributed to a cumulative effect related to nanoparticle internalization and time-dependent ion release. In summary, our results emphasize that the conditions during the impregnation step are critical to obtain functional textiles with a controlled release and an adequate biological response. This point is particularly relevant for wound-care applications, where the intended wearing time directly influences the textile's biocompatibility.

The selection of a cellulosic substrate allows the development of functional materials in a sustainable manner. Its simple and inexpensive production facilitates its access to a larger part of the population. In addition, obtaining stable support after sterilization processes offers the possibility of using it as a platform for the release of active substances according to the desired application.

Use of AI tools declaration

The authors declare that this article was produced without the use of Artificial Intelligence (AI) tools.

Conflict of interest

The authors declare no conflict of interest.

Acknowledgments

Nataly Arrieta-Sandoval acknowledges the National Council of Humanities, Science and Technology (CONAHCYT) for the financial support provided through the Estancias Posdoctorales por México 2023 program postdoctoral fellowship. The authors gratefully acknowledge the Universidad Autónoma de Ciudad Juárez (UACJ) for providing access to laboratory facilities for the synthesis and characterization of the materials.

Author contributions

NAS and JFHP: conceptualization and experimental design; NAS: investigation and experimental work; CARG and JFHP: supervision and project administration; IOA and LEVG: microbiology experiments and data analysis; NAS and CARG: preparation of figures and tables; NAS: manuscript preparation; JFHP and CARG: manuscript review and editing.

References

1. Ahmad W, Aquil Z, Alam SS (2020) Historical background of wound care. *Hamdan Med* 13: 189–195. https://doi.org/10.4103/HMJ.HMJ_37_20
2. Martínez-Correa E, Osorio-Delgado MA, Henao-Tamayo LJ, et al. (2020) Clasificación sistemática de apósitos: una revisión bibliográfica. *Revista mexicana de ingeniería biomédica* 41: 5–28. https://doi.org/10.17488/rmib.41.1.1
3. Sezer AD, Cevher E (2011) Biopolymers as wound healing materials: Challenges and new strategies, In: Pignatello R, *Biomaterials Applications for Nanomedicine*, London: InTech, 383–414. https://doi.org/10.5772/25177
4. Shalaby MA, Anwar MM, Saeed H (2022) Nanomaterials for application in wound healing: Current state-of-the-art and future perspectives. *J Polym Res* 29: 91. https://doi.org/10.1007/s10965-021-02870-x
5. Kim N, Lee S, Atala A (2013) Biomedical nanomaterials in tissue engineering, In: Gaharwar A, Sant S, Hancock M, et al. *Nanomaterials in Tissue Engineering*, Cambridge: Woodhead Publishing, 1–25e. https://doi.org/10.1533/9780857097231.1
6. Cao F, Wei C, Ma G, et al. (2021) Synthesis of photothermal antimicrobial cotton gauze using AuNPs as photothermal transduction agents. *RSC Adv* 11: 25976–25982. https://doi.org/10.1039/d1ra01597d
7. Liu G, Xiang J, Xia Q, et al. (2019) Superhydrophobic cotton gauze with durably antibacterial activity as skin wound dressing. *Cellulose* 26: 1383–1397. https://doi.org/10.1007/s10570-018-2110-y
8. Zhou L, Yu K, Lu F, et al. (2020) Minimizing antibiotic dosage through in situ formation of gold nanoparticles across antibacterial wound dressings: A facile approach using silk fabric as the base substrate. *J Clean Prod* 243: 118604. https://doi.org/10.1016/j.jclepro.2019.118604
9. Sathiyaseelan A, Saravanakumar K, Wang M (2022) Bimetallic silver-platinum (AgPt) nanoparticles and chitosan fabricated cotton gauze for enhanced antimicrobial and wound healing applications. *Int J Biol Macromol* 220: 1556–1569. https://doi.org/10.1016/j.ijbiomac.2022.09.045

10. Kim J, Kang SH, Choi Y, et al. (2023) Antibacterial and biofilm-inhibiting cotton fabrics decorated with copper nanoparticles grown on graphene nanosheets. *Sci Rep* 13: 11947. https://doi.org/10.1038/s41598-023-38723-4
11. Gonçalves RA, Ku JW, Zhang H, et al. (2022) Copper-nanoparticle-coated fabrics for rapid and sustained antibacterial activity applications. *ACS Appl Nano Mater* 5: 12876–12886. https://doi.org/10.1021/acsanm.2c02736
12. Chapa-González C, González-García L, Burciaga-Jurado L, et al. (2023) Bactericidal activity of silver nanoparticles in drug-resistant bacteria. *Braz J Microbiol* 54: 691–701. https://doi.org/10.1007/s42770-023-00991-7
13. Patel M, Kikani T, Saren U, et al. (2024) Bactericidal, anti-biofilm, anti-oxidant potency and catalytic property of silver nanoparticles embedded into functionalised chitosan gel. *Int J Biol Macromol* 262: 129968. https://doi.org/10.1016/j.ijbiomac.2024.129968
14. Gong X, Jadhav ND, Lonikar VV, et al. (2024) An overview of green synthesized silver nanoparticles towards bioactive antibacterial, antimicrobial and antifungal applications. *Adv Colloid Interface Sci* 323: 103053. https://doi.org/10.1016/j.cis.2023.103053
15. Aldakheel FM, Mohsen D, El Sayed MM, et al. (2023) Silver nanoparticles loaded on chitosan-g-PVA hydrogel for the wound-healing applications. *Molecules* 28: 3241. https://doi.org/10.3390/molecules28073241
16. Xu M, Ji X, Huo J, et al. (2023) Nonreleasing AgNP colloids composite hydrogel with potent hemostatic, photodynamic bactericidal and wound healing-promoting properties. *ACS Appl Mater Interfaces* 15: 17742–17756. https://doi.org/10.1021/acsami.3c03247
17. Diniz FR, Maia RCA, de Andrade LRM, et al. (2020) Silver nanoparticles-composing alginate/gelatine hydrogel improves wound healing in vivo. *Nanomaterials* 10: 390. https://doi.org/10.3390/nano10020390
18. Wang X, Wang Z, Fang S, et al. (2021) Injectable Ag nanoclusters-based hydrogel for wound healing via eliminating bacterial infection and promoting tissue regeneration. *Chem Eng J* 420: 127589. https://doi.org/10.1016/j.cej.2020.127589
19. El-Aassar M, Ibrahim OM, Fouda MM, et al. (2020) Wound healing of nanofiber comprising Polygalacturonic/Hyaluronic acid embedded silver nanoparticles: In-vitro and in-vivo studies. *Carbohydr Polym* 238: 116175. https://doi.org/10.1016/j.carbpol.2020.116175
20. Alven S, Buyana B, Feketshane Z, et al. (2021) Electrospun nanofibers/nanofibrous scaffolds loaded with silver nanoparticles as effective antibacterial wound dressing materials. *Pharmaceutics* 13: 964. https://doi.org/10.3390/pharmaceutics13070964
21. Mostafa M, Kandile NG, Mahmoud MK, et al. (2022) Synthesis and characterization of polystyrene with embedded silver nanoparticle nanofibers to utilize as antibacterial and wound healing biomaterial. *Heliyon* 8: e08872. https://doi.org/10.1016/j.heliyon.2022.e08772
22. Liu M, Liu T, Chen X, et al. (2018) Nano-silver-incorporated biomimetic polydopamine coating on a thermoplastic polyurethane porous nanocomposite as an efficient antibacterial wound dressing. *J Nanobiotechnol* 16: 1–19. https://doi.org/10.1186/s12951-018-0416-4
23. Brogliato AR, Borges PA, Barros JF, et al. (2014) The effect and safety of dressing composed by nylon threads covered with metallic silver in wound treatment. *Int Wound J* 11: 190–197. https://doi.org/10.1111/j.1742-481x.2012.01065.x

24. Mehta K, Kumar V, Rai B, et al. (2022) Development of cost effective, breathable & biocompatible nanosilver impregnated, acrylic acid grafted non-woven polypropylene (NWPP) wound dressing material with long lasting antimicrobial efficacy. *J Polym Res* 29: 191. https://doi.org/10.1007/s10965-022-03001-w
25. Gupta H, Verma C, Sharma A, et al. (2022) Development of silver immobilized biofunctional PET fabric for antimicrobial wound dressing. *J Polym Res* 29: 29. https://doi.org/10.1007/s10965-021–02844-z
26. Yuan S, Li J, Qi D, et al. (2023) Preparation of efficient and green silver-loaded viscose fabric and its antibacterial durability. *J Polym Environ* 31: 4069–4079. https://doi.org/10.1007/s10924-023–02844-8
27. Yang L, Jing Y, Zhou L, et al. (2025) Synthesis of viral-like lignin/Ag nanoparticles with spiky surfaces for antibacterial and antioxidant applications. *Int J Biol Macromol* 305: 141034. https://doi.org/10.1016/j.ijbiomac.2025.141034
28. Khansa I, Schoenbrunner AR, Kraft CT, et al. (2019) Silver in wound care—friend or foe?: A comprehensive review. *Plast Reconstr Surg Glob Open* 7: 2390. https://doi.org/10.1097/gox.0000000000002390
29. Foti A, Calì L, Petralia S, et al. (2023) Green nanoformulations of polyvinylpyrrolidone-capped metal nanoparticles: A study at the hybrid interface with biomimetic cell membranes and in vitro cell models. *Nanomaterials* 13: 1624. https://doi.org/10.3390/nano13101624
30. Neto FNS, Morais LA, Gorup LF, et al. (2023) Facile synthesis of PVP-coated silver nanoparticles and evaluation of their physicochemical, antimicrobial and toxic activity. *Colloids Interfaces* 7: 66. https://doi.org/10.3390/colloids7040066
31. Ortega-Córdova R, Sánchez-Carillo K, Carrasco-Saavedra S, et al. (2024) Polyvinylpyrrolidone-mediated synthesis of ultra-stable gold nanoparticles in a nonaqueous choline chloride–urea deep eutectic solvent. *RSC Appl Interfaces* 1: 600–611. https://doi.org/10.1039/D3LF00261F
32. Schultz G, Mozingo D, Romanelli M, et al. (2005) Wound healing and TIME; new concepts and scientific applications. *Wound Repair Regen* 13: 1–11. https://doi.org/10.1111/j.1067-1927.2005.1304s1.x
33. Abbasi AR, Morsali A (2011) Synthesis and properties of silk yarn containing Ag nanoparticles under ultrasound irradiation. *Ultrason Sonochem* 18: 282–287. https://doi.org/10.1016/j.ultsonch.2010.06.002
34. Moholkar VS (2002) Intensification of textile treatments: Sonoprocess engineering. Dissertation. Twente University. Available from: https://scispace.com/pdf/intensification-of-textile-treatments-sonoprocess-5ashh2qgdg.pdf.
35. Körlü A, Bahtiyari M (2021) Ultrasound-based wet processes in textile industry, In: Rather LJ, Haji A, Shabbir M, *Innovative and Emerging Technologies for Textile Dyeing and Finishing*, New York: Wiley, 265–299. https://doi.org/10.1002/9781119710288.ch10
36. Harifi T, Montazer M (2015) A review on textile sonoprocessing: A special focus on sonosynthesis of nanomaterials on textile substrates. *Ultrason Sonochem* 23: 1–10. https://doi.org/10.1016/j.ultsonch.2014.08.022
37. Gotoh K, Harayama K (2013) Application of ultrasound to textiles washing in aqueous solutions. *Ultrason Sonochem* 20: 747–753. https://doi.org/10.1016/j.ultsonch.2012.10.001

38. Tissera ND, Wijesena RN, de Silva KN (2016) Ultrasound energy to accelerate dye uptake and dye–fiber interaction of reactive dye on knitted cotton fabric at low temperatures. *Ultrason Sonochem* 29: 270–278. https://doi.org/10.1016/j.ultsonch.2015.10.002
39. Petkova P, Francesko A, Fernandes MM, et al. (2014) Sonochemical coating of textiles with hybrid ZnO/chitosan antimicrobial nanoparticles. *ACS Appl Mater Interfaces* 6: 1164–1172. https://doi.org/10.1021/am404852d
40. Martinaga Pintarić L, Somogi Škoc M, Ljoljić Bilić V, et al. (2020) Synthesis, modification and characterization of antimicrobial textile surface containing ZnO nanoparticles. *Polymers* 12: 1210. https://doi.org/10.3390/polym12061210
41. Silva DJ, Barbosa RF, Souza AG, et al. (2022) Morphological, UV blocking, and antimicrobial features of multifunctional cotton fibers coated with ZnO/Cu via sonochemistry. *Mater Chem Phys* 286: 126210. https://doi.org/10.1016/j.matchemphys.2022.126210
42. Li Q, Zhang N, Ni L, et al. (2021) One-pot high efficiency low temperature ultrasonic-assisted strategy for fully bio-based coloristic, anti-pilling, antistatic, bioactive and reinforced cashmere using grape seed proanthocyanidins. *J Clean Prod* 315: 128148. https://doi.org/10.1016/j.jclepro.2021.128148
43. Baggini SP (2022) Sterilization in microbiology. *Medicon Microbiol* 1: 23–29. Available from: https://themedicon.com/pdf/mcmi/MCMI-22-010.pdf.
44. Chen WC, Ko CY, Chang KC, et al. (2022) Preparation of electrospun silver/poly(vinyl alcohol) fibrous membranes and characterization of the effect of sterilization processes on the antibacterial activity. *J Ind Text* 51: 7205S–7222S. https://doi.org/10.1177/1528083720913345
45. Zheng J, Clogston JD, Patri AK, et al. (2011) Sterilization of silver nanoparticles using standard gamma irradiation procedure affects particle integrity and biocompatibility. *J Nanomed Nanotechnol* 2011: 001. https://doi.org/10.4172/2157-7439.S5-001
46. França A, Pelaz B, Moros M, et al. (2010) Sterilization matters: Consequences of different sterilization techniques on gold nanoparticles. *Small* 6: 89–95. https://doi.org/10.1002/smll.200901006
47. Kokubo T, Takadama H (2006) How useful is SBF in predicting in vivo bone bioactivity? *Biomaterials* 27: 2907–2915. https://doi.org/10.1016/j.biomaterials.2006.01.017
48. Montes-Hernandez G, Di Girolamo M, Sarret G, et al. (2021) In situ formation of silver nanoparticles (Ag-NPs) onto textile fibers. *ACS Omega* 6: 1316–1327. https://doi.org/10.1021/acsomega.0c04814
49. Čuk N, Šala M, Gorjanc M (2021) Development of antibacterial and UV protective cotton fabrics using plant food waste and alien invasive plant extracts as reducing agents for the in-situ synthesis of silver nanoparticles. *Cellulose* 28: 3215–3233. https://doi.org/10.1007/s10570-021-03715-y
50. Chen H, Zhang G, Zhang W, et al. (2023) Silver nanoparticles deposited on a cotton fabric surface via an in situ method using reactive hyperbranched polymers and their antibacterial properties. *RSC Adv* 13: 11450–11456. https://doi.org/10.1039/D3RA00989K
51. Abidi N, Cabrales L, Haigler C (2014) Changes in the cell wall and cellulose content of developing cotton fibers investigated by FTIR spectroscopy. *Carbohydr Polym* 100: 9–16. https://doi.org/10.1016/j.carbpol.2013.01.074
52. Souza JM, Henriques M, Teixeira P, et al. (2019) Comfort and infection control of chitosan-impregnated cotton gauze as wound dressing. *Fibers Polym* 20: 922–932. https://doi.org/10.1007/s12221-019-9053-2

53. Abidi N, Hequet E, Cabrales L, et al. (2008) Evaluating cell wall structure and composition of developing cotton fibers using Fourier transform infrared spectroscopy and thermogravimetric analysis. *J Appl Polym Sci* 107: 476–486. https://doi.org/10.1002/app.27100
54. Ilharco LM, Garcia AR, Lopes da Silva J, et al. (1997) Infrared approach to the study of adsorption on cellulose: Influence of cellulose crystallinity on the adsorption of benzophenone. *Langmuir* 13: 4126–4132. https://doi.org/10.1021/la962138u
55. Selvam S, Sundrarajan M (2012) Functionalization of cotton fabric with PVP/ZnO nanoparticles for improved reactive dyeability and antibacterial activity. *Carbohydr Polym* 87: 1419–1424. https://doi.org/10.1016/j.carbpol.2011.09.025
56. Zhao T, Sun R, Yu S, et al. (2010) Size-controlled preparation of silver nanoparticles by a modified polyol method. *Colloids Surf A Physicochem Eng Asp* 366: 197–202. https://doi.org/10.1016/j.colsurfa.2010.06.005
57. Klemm D, Heublein B, Fink HP, et al. (2005) Cellulose: Fascinating biopolymer and sustainable raw material. *Angew Chem Int Ed* 44: 3358–3393. https://doi.org/10.1002/anie.200460587
58. Ferro M, Mannu A, Panzeri W, et al. (2020) An integrated approach to optimizing cellulose mercerization. *Polymers* 12: 1559. https://doi.org/10.3390/polym12071559
59. Sarkar S, Das R (2018) Shape effect on the elastic properties of Ag nanocrystals. *Micro Nano Lett* 13: 312–315. https://doi.org/10.1049/mnl.2017.0349
60. Haaf F, Sanner A, Straub F (1985) Polymers of N-vinylpyrrolidone: Synthesis, characterization and uses. *Polym J* 17: 143–152. Available from: https://scispace.com/pdf/polymers-of-n-vinylpyrrolidone-synthesis-characterization-rcywz1qmcu.pdf.
61. Süvegh K, Zelkó R (2002) Physical aging of poly(vinylpyrrolidone) under different humidity conditions. *Macromolecules* 35: 795–800. https://doi.org/10.1021/ma011148l
62. Fitzpatrick S, McCabe JF, Petts CR, et al. (2002) Effect of moisture on polyvinylpyrrolidone in accelerated stability testing. *Int J Pharm* 246: 143–151. https://doi.org/10.1016/s0378-5173(02)00375-7
63. Bhattacharya S, Sharma DK, Saurabh S, et al. (2013) Plasticization of poly(vinylpyrrolidone) thin films under ambient humidity: Insight from single-molecule tracer diffusion dynamics. *J Phys Chem B* 117: 7771–7782. https://doi.org/10.1021/jp401704e
64. Bristi UL, Rahman A, Malitha SB, et al. (2024) Modification of cotton gauze using Cynodon dactylon (Bermuda grass) and assessment of the chemical and antimicrobial properties. *Sci Rep* 14: 31650. https://doi.org/10.1038/s41598-024-80318-0
65. Xiang J, Zhu R, Lang S, et al. (2021) Mussel-inspired immobilization of zwitterionic silver nanoparticles toward antibacterial cotton gauze for promoting wound healing. *Chem Eng J* 409: 128291. https://doi.org/10.1016/j.cej.2020.128291
66. Li Petri G, Facchiano S, Trovato V, et al. (2025) Antibacterial activity of textiles functionalized with silversil. *ChemNanoMat* 11: 2500132. https://doi.org/10.1002/cnma.202500132
67. Blosi M, Brigliadori A, Ortelli S, et al. (2024) Re-designing nano-silver technology exploiting one-pot hydroxyethyl cellulose-driven green synthesis. *Front Chem* 12: 1432546. https://doi.org/10.3389/fchem.2024.1432546
68. Gao M, Sun L, Wang Z, et al. (2013) Controlled synthesis of Ag nanoparticles with different morphologies and their antibacterial properties. *Mater Sci Eng C* 33: 397–404. https://doi.org/10.1016/j.msec.2012.09.005

69. Pazos-Ortiz E, Roque-Ruiz JH, Hinojos-Márquez EA, et al. (2017) Dose-dependent antimicrobial activity of silver nanoparticles on polycaprolactone fibers against gram-positive and gram-negative bacteria. *J Nanomater* 2017: 4752314. https://doi.org/10.1155/2017/4752314
70. Zein R, Alghoraibi I, Soukkarieh C, et al. (2022) Influence of polyvinylpyrrolidone concentration on properties and anti-bacterial activity of green synthesized silver nanoparticles. *Micromachines* 13: 777. https://doi.org/10.3390/mi13050777
71. Liu W, Fourmy D, Dragoe D, et al. (2025) Radiation-induced synthesis of silver nanocomposites and their antibacterial applications. *Sci Rep* 15: 40570. https://doi.org/10.1038/s41598-025-24235-w
72. Bondarenko O, Ivask A, Käkinen A, et al. (2013) Particle-cell contact enhances antibacterial activity of silver nanoparticles. *PLoS One* 8: e64060. https://doi.org/10.1371/journal.pone.0064060
73. Ahmad SA, Das SS, Khatoon A, et al. (2020) Bactericidal activity of silver nanoparticles: A mechanistic review. *Mater Sci Energy Technol* 3: 756–769. https://doi.org/10.1016/j.mset.2020.09.002
74. Bruna T, Maldonado-Bravo F, Jara P, et al. (2021) Silver nanoparticles and their antibacterial applications. *Int J Mol Sci* 22: 7202. https://doi.org/10.3390/ijms22137202
75. Sati A, Ranade TN, Mali SN, et al. (2025) Silver nanoparticles (AgNPs): Comprehensive insights into bio/synthesis, key influencing factors, multifaceted applications, and toxicity—A 2024 update. *ACS Omega* 10: 7549–7582. https://doi.org/10.1021/acsomega.4c11045
76. Skomorokhova EA, Sankova TP, Orlov IA, et al. (2020) Size-dependent bioactivity of silver nanoparticles: Antibacterial properties, influence on copper status in mice, and whole-body turnover. *Nanotechnol Sci Appl* 13: 137–157. https://doi.org/10.2147/NSA.S287658
77. Ru J, Qian X, Wang Y (2018) Study on antibacterial finishing of cotton fabric with silver nanoparticles stabilized by nanoliposomes. *Cellulose* 25: 5443–5454. https://doi.org/10.1007/s10570-018-1953-6
78. Raja A, Thilagavathi G, Kannaian T, et al. (2010) Synthesis of spray dried polyvinyl pyrrolidone coated silver nanopowder and its application on wool and cotton for microbial resistance. *Indian J Fibre Text Res* 35: 59–64. Available from: https://nopr.niscair.res.in/handle/123456789/7671.
79. Ribeiro AI, Senturk D, Silva KK, et al. (2019) Antimicrobial efficacy of low concentration PVP-silver nanoparticles deposited on DBD plasma-treated polyamide 6, 6 fabric. *Coatings* 9: 581. https://doi.org/10.3390/coatings9090581
80. Ribeiro AI, Modic M, Cvelbar U, et al. (2020) Effect of dispersion solvent on the deposition of PVP-silver nanoparticles onto DBD plasma-treated polyamide 6, 6 fabric and its antimicrobial efficiency. *Nanomaterials* 10: 607. https://doi.org/10.3390/nano10040607
81. Vigneshwaran N, Kathe A, Varadarajan P, et al. (2007) Functional finishing of cotton fabrics using silver nanoparticles. *J Nanosci Nanotechnol* 7: 1893–1897. https://doi.org/10.1166/jnn.2007.737
82. Chen WC, Ko CY, Chang KC, et al. (2020) Influences of processing and sterilizing strategies on reduced silver nanoparticles in poly(vinyl alcohol) electrospun membranes: Optimization and preservation of antibacterial activity. *Mater Chem Phys* 254: 123300. https://doi.org/10.1016/j.matchemphys.2020.123300

83. Ambi A, Wakte P, Bhusari S, et al. (2025) Development and validation of UV-Visible spectrophotometric method for estimation of dexlansoprazole. *J Drug Deliv Ther* 15: 148–155. https://doi.org/10.22270/jddt.v15i8.7332
84. Gurina D, Surov O, Voronova M, et al. (2019) Water effects on molecular adsorption of poly(N-vinyl-2-pyrrolidone) on cellulose nanocrystals surfaces: Molecular dynamics simulations. *Materials* 12: 2155. https://doi.org/10.3390/ma12132155
85. Struik GM, Vrijland WW, Birnie E, et al. (2018) A randomized controlled trial on the effect of a silver carboxymethylcellulose dressing on surgical site infections after breast cancer surgery. *PLoS One* 13: 0195715. https://doi.org/10.1371/journal.pone.0195715
86. Kaya M, Akdaşçi E, Eker F, et al. (2025) Recent advances of silver nanoparticles in wound healing: Evaluation of in vivo and in vitro studies. *Int J Mol Sci* 26: 9889. https://doi.org/10.3390/ijms26209889
87. Nešporová K, Pavlík V, Šafránková B, et al. (2020) Effects of wound dressings containing silver on skin and immune cells. *Sci Rep* 10: 15216. https://doi.org/10.1038/s41598-020-72249-3
88. Rónavári A, Bélteky P, Boka E, et al. (2021) Polyvinyl-pyrrolidone-coated silver nanoparticles—The colloidal, chemical, and biological consequences of steric stabilization under biorelevant conditions. *Int J Mol Sci* 22: 8673. https://doi.org/10.3390/ijms22168673
89. Kang K, Jung H, Lim JS, et al. (2012) Cell death by polyvinylpyrrolidine-coated silver nanoparticles is mediated by ROS-dependent signaling. *Biomol Ther (Seoul)* 20: 399–405. https://doi.org/10.4062/biomolther.2012.20.4.399
90. Pourhoseini S, Enos RT, Murphy AE, et al. (2021) Characterization, bio-uptake and toxicity of polymer-coated silver nanoparticles and their interaction with human peripheral blood mononuclear cells. *Beilstein J Nanotechnol* 12: 282–294. https://doi.org/10.3762/bjnano.12.23
91. Sindhi K, Pingili RB, Beldar V, et al. (2025) The role of biomaterials-based scaffolds in advancing skin tissue construct. *J Tissue Viability* 34: 100858. https://doi.org/10.1016/j.jtv.2025.100858
92. Krishani M, Shin WY, Suhaimi H, et al. (2023) Development of scaffolds from bio-based natural materials for tissue regeneration applications: A review. *Gels* 9: 100. https://doi.org/10.3390/gels9020100
93. Fayer L, Vasconcellos R, de Oliveira ER, et al. (2024) Cotton cellulose nanofiber/chitosan scaffolds for skin tissue engineering and wound healing applications. *Biomed Mater* 20: 015024. https://doi.org/10.1088/1748-605x/ad9da4
94. Li X, Sim D, Wang Y, et al. (2025) Fiber-based biomaterial scaffolds for cell support towards the production of cultivated meat. *Acta Biomater* 191: 292–307. https://doi.org/10.1016/j.actbio.2024.11.006
95. Andleeb A, Dikici S, Waris TS, et al. (2020) Developing affordable and accessible pro-angiogenic wound dressings; incorporation of 2 deoxy D-ribose (2dDR) into cotton fibres and wax-coated cotton fibres. *J Tissue Eng Regen Med* 14: 973–988. https://doi.org/10.1002/term.3072
96. Tallapaneni V, Kalaivani C, Pamu D, et al. (2021) Acellular scaffolds as innovative biomaterial platforms for the management of diabetic wounds. *Tissue Eng Regen Med* 18: 713–734. https://doi.org/10.1007/s13770-021-00344-1

AIMS Press